

Delivery of encapsulated green fluorescent protein plasmid and mRNA to human embryonic
kidney cells using Aqueous Partitioning Capsules

by

Shelby Innes

B.S., Emporia State University, 2021

A THESIS

submitted in partial fulfillment of the requirements for the degree

MASTER OF SCIENCE

Department of Biochemistry and Molecular Biophysics
College of Arts and Sciences

KANSAS STATE UNIVERSITY
Manhattan, Kansas

2023

Approved by:

Major Professor
John M. Tomich

Copyright

© Shelby Innes 2023.

Abstract

Aqueous Partitioning Capsules (APC) are a novel delivery system generated from peptides with a primary sequence of Ac-KKKFLIVIKKK-COHN₂. Transmission electron microscopy of APC revealed that the peptides formed a spherical shape at a pH of 2. Therefore, the peptide (Ac-KKKFLIVIKKK-COHN₂), at a pH of 2, was considered as a possible mRNA delivery system. Circular dichroism data shows that the peptides form random coils at pH 2 and 7, and forms β -sheets at pH 12. The size characteristics of APC were determined using dynamic light scattering (DLS) and nanoparticle tracking analysis. APC have been shown to encapsulate rhodamine 6G dye and genetic materials, such as green fluorescent protein (GFP) plasmid and mRNA. GFP-encoding mRNA and plasmid were encapsulated, as well as attached to the outside of APC. To determine the location of the genetic materials, RiboGreenTM assays and nuclease digestion studies were used to confirm the location of the genetic material, on either the outside (accessible) or the inside (protected) of APC. APC have shown efficiency in delivering GFP plasmids and GFP mRNA for transfection of human embryonic kidney (HEK) cells. The stability of APC were studied over time using DLS to measure any size changes. Preliminary studies of APC encapsulation abilities, stability over time, and delivery of GFP mRNA and plasmid to HEK cells will be discussed.

Table of Contents

Abbreviations	vi
List of Figures	vii
List of Tables	ix
Acknowledgements	x
Dedication	xi
Chapter 1 - Introduction and Background	1
Nanotechnology	1
Liposomes	3
Polymersomes	4
Branched Amphiphilic Peptide Capsules	5
Corralling Amphipathic Peptide Colloids	7
Aqueous Partitioning Capsules	8
Chapter 2 - Characteristics of APC	11
Materials and Methods	11
Peptide Synthesis	11
Preparation of APC	13
Preparation of mRNA- or dsDNA-APC's nanoparticles	14
Circular dichroism	14
Dynamic light scattering and zeta potential characterization	15
Nanoparticle Tracking Analysis	16
Results and Discussion	17
Circular Dichroism	17
Dynamic Light Scattering	21
Nanoparticle Tracking Analysis	26
Discussion	28
Chapter 3 - Delivery and Encapsulation of Genetic Materials and Dyes Using APC	29
Materials and Methods	29
APC dye encapsulation	29
APC GFP plasmid and GFP mRNA transfections	30

RiboGreen Assays.....	32
Gel Electrophoresis.....	32
Nanoparticle Tracking Analysis	33
Results and Discussion	34
Encapsulation of Rhodamine 6G Dye.....	34
GFP Plasmid Transfections Using APC	35
GFP mRNA Transfections Using APC.....	39
RiboGreen Assays.....	49
Gel Electrophoresis	50
NTA Characterization of APC with Genetic Materials	52
Chapter 4 - Stability of APC.....	54
Materials and Methods.....	54
Time Stability Studies.....	54
Results and Discussion	55
Time Stability of APC	55
Chapter 5 - Discussion and Future Work.....	59
Discussion.....	59
Future Work.....	61
References.....	65

Abbreviations

AAV.....	Adeno-associated viruses
APC.....	Aqueous Partitioning Capsules
BAPC.....	Branched Amphiphilic Peptide Capsules
BHK.....	Baby hamster kidney
CAPC.....	Corralling Amphipathic Peptide Colloids
CD.....	Circular dichroism
CF.....	Cystic fibrosis
DAPI.....	4',6'-diamidino-2-phenylindole
DCM.....	Dichloromethane
DLS.....	Dynamic light scattering
DMF.....	Dimethylformamide
FBS.....	Fetal bovine serum
FRET.....	Fluorescence resonance energy transfer
GFP.....	Green fluorescent protein
HATU.....	1-[Bis(dimethylamino)methylene]-1H-1,2,3-triazolo[4,5-b]pyridinium 3-oxid hexafluorophosphate
HEK.....	Human embryonic kidney
HoAT.....	1-Hydroxy-7-azabenzotriazole
NMP.....	N-Methyl-2-pyrrolidone
PBS.....	Phosphate buffer saline
PFA.....	Perfluoroalkoxy alkanes
PSI.....	Pounds per square inch
TE.....	Tris/EDTA
TEM.....	Transmission electron microscopy
TFA.....	Trifluoroacetic acid
TFE.....	2,2,2-Trifluoroethanol

List of Figures

Figure 1.1. BAPC h ₅ and h ₉ peptide sequences	5
Figure 1.2. K ₃ h _{5n} K ₃ peptide forms nanospheres at pH 2, different structures at higher pH.....	8
Figure 2.1. K ₃ h _{5n} K ₃ peptide forms random coils at acidic and neutral pH, β-sheets at basic pH. 18	
Figure 2.2. TFE induces secondary structure change in K ₃ h _{5n} K ₃ peptides from random coils to α-helices	19
Figure 2.3. K ₃ h ₅ K ₃ and K ₃ h ₉ K ₃ peptide forms random coils at acidic and neutral pH.....	21
Figure 2.4. NTA reveals size distribution profile of APC formulated at pH 2, showing particle size between 100-200 nm.....	26
Figure 2.5. NTA reveals size distribution profile of APC formulated at pH 3, showing particle size between 200-700 nm.....	27
Figure 3.1. APC encapsulates rhodamine 6G dye	34
Figure 3.2. Human embryonic kidney cells treated with either no transfection reagent or Lipofectamine 3000™ complexed with GFP plasmid.....	36
Figure 3.3. APC deliver surface-bound GFP plasmid to HEK cells.....	37
Figure 3.4. APC deliver encapsulated GFP plasmid to HEK cells.....	38
Figure 3.5. Human embryonic kidney cells treated with either no transfection reagent or Lipofectamine MessengerMAX™ complexed with GFP mRNA	40
Figure 3.6. APC deliver surface-bound GFP mRNA to HEK cells.....	41
Figure 3.7. APC deliver encapsulated GFP mRNA to HEK cells	42
Figure 3.8. Cell viability of human embryonic kidney cells treated with no transfection reagent and Lipofectamine MessengerMAX.....	43
Figure 3.9. APC, formulated from K ₃ h _{5n} K ₃ peptide, deliver GFP mRNA to HEK cells without affecting cell viability	44
Figure 3.10. APC, formulated from K ₃ h ₅ K ₃ peptide, deliver GFP mRNA to HEK cells without affecting cell viability	45
Figure 3.11. APC, formulated from K ₃ h ₉ K ₃ peptide, deliver GFP mRNA and GFP plasmid to BHK cells.....	46
Figure 3.12. APC deliver GFP mRNA to HEK cells.....	48

Figure 3.13. RiboGreen assay reveals differences in fluorescence between APC with surface-bound versus encapsulated DNA	50
Figure 3.14. APC protects DNA from DNase digestion.....	51
Figure 3.15. NTA reveals size distribution profile of APC with encapsulated DNA forms particles ranging 100-400 nm in size	52
Figure 3.16. NTA reveals size distribution profile of APC with surface-bound DNA forms particles ranging 100-500 nm in size	53
Figure 5.1. APC formulation process	59
Figure 5.2. Proposed structure of assembled APC in aqueous solvents	60
Figure 5.3. Delivery of dyes to cystic fibrosis cells using APC and CAPC.....	63

List of Tables

Table 1.1. APC peptide sequences.....	10
Table 2.1. DLS shows APC sizes increase as pH is increased	21
Table 2.2. APC form nanosized particles when formed at pH of 3.51 and below (5-minute incubation)	23
Table 2.3. APC form nanosized particles when formed at pH of 3.51 and below (20-minute incubation)	24
Table 2.4. APC formulated from K ₃ h ₅ K ₃ peptides exhibit similar trends in particle size as APC formulated from K ₃ h _{5n} K ₃ peptides.....	25
Table 2.6. APC formulated from K ₃ h ₉ K ₃ peptides exhibit similar trends in particle size as APC formulated from K ₃ h _{5n} K ₃ peptides.....	25
Table 3.1. APC complexed with GFP plasmid form particles between 100-300 nm in size.....	39
Table 4.1. APC, formulated from K ₃ h _{5n} K ₃ , shows size instability when stored at room temperature (25°C).....	55
Table 4.2. APC, formulated from K ₃ h _{5n} K ₃ , shows size instability when stored 4°C	56
Table 4.3. APC, formulated from K ₃ h ₉ K ₃ , shows size instability when stored at room temperature (25°C).....	57
Table 4.4. Size stability of APC, formulated from K ₃ h ₉ K ₃ , when stored at 4°C, tracked over the course of 20 days	58

Acknowledgements

I would first like to thank my major professor, Dr. John Tomich. He has helped my knowledge of biochemistry, as well as nanotechnology, greatly expand throughout my time at Kansas State University. He has helped equip me with improved research skills that will help as I continue my education and career in academia. I would also like to thank my committee members- Dr. Bruce Schultz and Dr. Erika Giesbrecht for their useful suggestions in ways to improve my research project.

I am grateful for current and past members of Dr. John Tomich's lab. Especially Susan Whitaker, who taught me a great wealth of knowledge about peptide chemistry and the instruments used in the lab. She has helped me improve as greatly as a researcher and upheld my love for laboratory work. I would also like to thank former lab members, Drs. Pinakin Sukthankar and Sheila Barros. I am also grateful for current and former undergraduate and graduate students who have helped contribute to my project: Taryn Lubber, Hannah Long, Kotis Anderson, and Sungmin Yoon. I would also like to thank our former and current research technicians: Ted Moser and Iryna Graham.

Dedication

I would like to dedicate this work to my family and friends who continually give me their support and help drive my ambition to pursue higher education.

Chapter 1 - Introduction and Background

Nanotechnology

Nanotechnology as applied to therapeutics, known as nanomedicine yields many possibilities in healthcare.¹ Nanotechnology is defined as particles or capsules having a size of 100 nm or less.^{2,3} Nanomedicine encompasses a slightly larger range of nanodrugs with sizes up to or above 200 nm.² One major aspect of nanomedicine is delivery of drugs and genetic materials into cells. Throughout the past decade, the field of nanotechnology and its applications in medicine have grown greatly. For example, nanotechnology has opened the door to promising treatments for genetic diseases and cancers.⁴⁻⁷ Nanotechnology has improved delivery systems of drugs and genetic materials through increasing the stability, increasing half-life, increasing the solubility for hydrophobic drugs, and aiding in controlled release.¹ With the delivery of genetic material in particular, the use of nanotechnology has shown to be useful in aiding in vaccine delivery, as seen with the mRNA-based SARS-CoV-2 vaccines made by Moderna and BioNTech/Pfizer.^{2,8,9}

The delivery of genetic material and gene therapy drugs face many challenges that are not present in other therapies; including being degraded within the bloodstream, high immunogenicity, poor cellular uptake, and low release efficiency.^{4,10-12} Poor cellular uptake of genetic materials stems from their polyanionic structures, which make them unable to penetrate the nonpolar cell membranes or tissue barriers.¹³ mRNA, specifically, is more difficult to deliver into cells when compared to DNA and double-stranded RNA (dsRNA) because it is less stable in storage or circulation.

A delivery system for genetic materials and gene therapy drugs can overcome current barriers and improve effectiveness of these therapies.^{7,10} Two types of FDA approved vectors

include viral and nonviral vectors.^{4,14,15} Some commonly used viral vectors include adeno-associated viruses (AAV), retroviruses, and lentiviruses.^{4,16,17} Viral vectors are able to efficiently deliver many different types of genetic materials, however, they are more likely to be toxic to cells and elicit immune responses. One example of a currently used viral vector delivery system is with the Johnson & Johnson DNA SARS-CoV-2 vaccine. This vaccine uses AAV to deliver DNA encoding for the SARS-CoV-2 S protein.^{18,19} Problems arising from viral vectors include complex manufacturing processes and eliciting an immune response.^{16,20,21} Manufacturing of viral vectors requires many steps to scale up production to meet market demands.^{20,21} Production of AAV includes plasmid development, cell expansion, and viral vector production and purification.²⁰ These processes are costly, time-consuming, and require multiple steps.

Nonviral vectors can include lipid, polymer, and peptide nanoparticles.^{4,6,9,10} Lipid vectors for gene delivery are more biocompatible and less likely to elicit immune responses than viral vectors but are less efficient at gene delivery.²²⁻²⁴ Examples of lipid nanoparticles being used as a delivery system is with the Moderna and BioNTech/Pfizer SARS-CoV-2 vaccines. These vaccines contain nucleoside-modified mRNA, encoding for the SARS-CoV-2 S protein, held within lipid nanoparticles to allow for delivery of the genetic material to cells.²⁵ Polymeric nanoparticles, specifically cationic polymers, show promise for gene delivery due to their positive charges neutralizing the negatively charged genetic materials and their modifiable chemical structures that allow for increased carrying capacity.^{15,26,27} Compared to liposomal drug delivery systems, polymeric delivery systems have been shown to increase stability of the material being delivered and aid in creating controlled release systems.^{1,23,24} For mRNA delivery, specifically, nonviral vectors are the preferred delivery vehicles, due to their ability to protect

mRNA from degradation while exhibiting lower immunogenicity and easier manufacturing processes than viral vectors.^{22,23}

Liposomes

Lipid delivery vectors, or liposomes, are the most commonly used nanoparticle for delivery, with multiple formulations gaining FDA approval.^{15,28} Liposomes are composed of a lipid bilayer that can self-assemble in aqueous solvents and complex together with solutes, such as drugs and genetic materials.²⁹ The SARS-CoV-2 vaccines by Moderna and BioNTech/Pfizer employed liposomes to complex with and deliver mRNA-encoding for the SARS-CoV-2 S protein.^{8,9,19} Liposomes for these vaccines are comprised of a lipid bilayer that carries a cationic surface charge, allowing it to complex with the negatively charged mRNA.¹⁹ mRNA-liposomal complexes carry a neutral charge, which allows for penetration of cell membranes to deliver the genetic material.^{19,30}

Two examples of commercially available liposomal transfection reagents are Lipofectamine 3000™ and Lipofectamine MessengerMAX™. Both of these reagents are capable of delivering genetic materials to a wide-range of cells, including primary cultures, stem cells, and cancer cells.^{30,31} Lipofectamine™ transfection reagents consist of a cationic head groups, hydrocarbon tails consisting of 14 or more carbon atoms, spacer groups connecting the head groups to the hydrocarbon tails, and helper lipids.³⁰ The helper lipid is a neutral co-lipid that complexes with the cationic lipid and aids in formulation of complexes with genetic materials.³⁰ The positively charged Lipofectamine™ reagents complex together with negatively charged genetic materials, allowing for delivery of genetic materials across cell membranes. Lipofectamine 3000™ is designed specifically for DNA and dsRNA delivery, while Lipofectamine MessengerMAX™ is designed specifically mRNA delivery to cells. Both

liposomal reagents can efficiently deliver genetic materials to cells efficiently. However, drawbacks include cytotoxicity and difficult manufacturing processes that result in high costs.^{30,32}

Conjugation or encapsulation of amphiphilic peptides with liposomes has improved their usefulness in nanomedicine, specifically in the treatment of cancers.^{29,33} Through conjugation with targeting peptides, the liposomes can target cancer cells selectively.^{33,34} Liposomes are highly successful in delivering genetic material and aiding in therapeutic treatments, however, some limitations include the potential to alter the pharmacological effects of drugs, along with unknown stability and difficult preparation processes.

Polymersomes

Polymeric nanoparticles, or polymerosomes, are made of repeating units of various polymers, with common constituents being polyethylene glycol and chitin.^{35,36} Polymeric nanoparticles are classified as either non-biodegradable or biodegradable. Biodegradable polymeric nanoparticles are less cytotoxic than non-biodegradable polymeric nanoparticles, making them more commonly used for therapeutic purposes.^{15,26,27} The modifiable structure of both non-biodegradable and biodegradable polymeric nanoparticles allow them to have multiple therapeutic uses; such as altering surface properties of the nanoparticles for cellular targeting or carrying different drugs or genetic materials.^{26,35,36} Still, the major limitations to these nanotechnologies include difficult and complex manufacturing processes, intracellular biodegradability, and short half-lives in biological systems.^{26,37}

Branched Amphiphilic Peptide Capsules

Self-assembling nano-carriers show promise as delivery vehicles, as they can overcome obstacles such as poor absorption that can be seen in other drug delivery classes.^{38,39}

Biomolecular self-assembly occurs frequently in nature, such as many of the multi-protein complexes that are needed for cellular functions.³⁸⁻⁴⁰ Developing self-assembling nano-carriers using

biomolecules, such as peptides, shows promise in improving delivery of drugs and genetic materials.^{36,38,41-43} Biomolecular self-assembly is described as the spontaneous process forming noncovalent interactions resulting in an ordered 3D structure, with no external guidance to aid the assembly process.^{38,44,45} Self-assembly of peptide nano-carriers will typically occur due to a small change in the environment, such as pH or temperature, which alters the peptides in a way that promotes the formation of new ordered 3D structure, due to novel noncovalent interactions.^{38,46} Self-assembling nano-carriers will typically have simple, one-step assembly processes, overcoming a hurdle of other nanotechnologies that require complex and costly manufacturing processes.¹⁴

Branched amphiphilic peptide capsules (BAPC) are self-assembling peptide-based nanoparticles.^{14,24,47-49} BAPC are formulated using two distinct branched, amphiphilic peptides, h₅ and h₉, shown in **Figure 1.1**. BAPC are self-assembled peptide-based nanoparticles that form in water at room temperature.^{44,49} As compared to other types of nanotechnologies, BAPC have simple formulation processes, requiring only a single-step hydration. Along with a simple

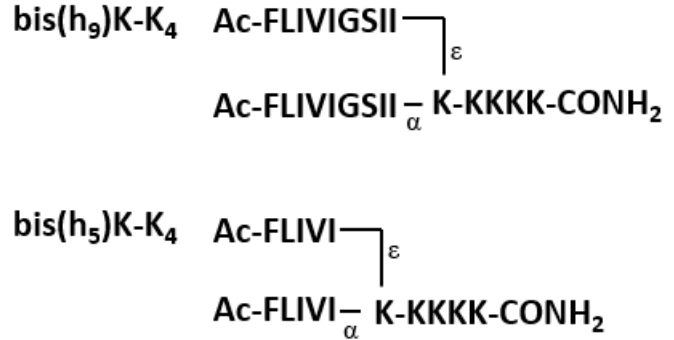


Figure 1.1. BAPC h₅ and h₉ peptide sequences. The two branched peptide sequences used, in equimolar concentrations, to formulate BAPC.

formulation process, BAPC are composed of peptides and mimic the structure of biomolecules; both characteristics that decrease the possibility of immunogenicity.^{24,44} BAPC have been shown previously to maintain their self-assembled structures at temperatures up to 37°C.⁴⁹ Previous research has shown delivery of plasmid DNA and dsRNA to cells using BAPC as the delivery system.⁵⁰⁻⁵²

BAPC were first described in Gudlur et al.⁴⁴, who described the initial discovery that these peptides self-assembled into nanovesicles. After initial discovery of the self-assembling nature of BAPC, they were studied for their ability to deliver various solutes and genetic materials into cells. In a study by Avila et al.⁵⁰, BAPC were shown to be efficient in facilitating delivery of lethal dsRNA to red flour beetles (*Tribolium castaneum*) and pea aphids (*Acyrtosiphon pisum*). The dsRNA was bound to BAPC surfaces and delivered orally through their diets.⁵⁰ Ingestion of the lethal dsRNA/BAPC complexes by both insect species resulted in death and demonstrated that BAPC were able to deliver genetic material via oral inoculation.⁵⁰ In a study by Avila et al.⁵³, BAPC were shown to deliver plasmid DNA both *in vitro* and *in vivo*. *In vitro*, BAPC were used to transfect HeLa cells with plasmid encoding for GFP and *in vivo*, BAPC delivered HPV-16 oncogene encoding DNA vaccines to mice.⁵³ Inoculation of the mice with the DNA/BAPC complexes resulted in efficient tumor growth control compared to mice receiving no vaccine treatment, or naked DNA (not complexed with BAPC).⁵³

BAPC have very simple assembly processes, initially both the h₅ and h₉ peptides (**Figure 1.1.**) are dissolved individually in trifluoroethanol (TFE), combined in an equimolar ratio, dried using vacuum suction, and rehydrated using deionized water or an aqueous solution containing a solute.^{14,44} TFE is used to dissolve the individual peptides, since the h₅ and h₉ peptides form α -helices when in this hydrophobic solvent, meaning the peptides are unable to form capsules

under these conditions. This ensures capsules are not formed until both peptides are combined. This simple formation process allows for efficient formulation and less room for quality control errors that may occur with complex manufacturing processes. Along with a simple formulation process, BAPC are stable at high temperatures (37°C), when exposed to proteases, and when exposed to chaotropes.^{14,49} BAPC stability can be both an advantage and disadvantage for them as cargo delivery. An advantage is that BAPC are stable at higher temperatures, such as body temperature, and when exposed to a wide range of chemical agents, which allows for encapsulation of a wide range of solutes. However, a disadvantage of high stability is that BAPC sometimes have a lowered efficiency of cargo delivery once inside cells.¹⁴ That being said, BAPC have been shown to deliver multiple types of solutes, including genetic materials into cells.

Corralling Amphipathic Peptide Colloids

Another example of a self-assembling peptide-based nanoparticle are Corralling Amphipathic Peptide Colloids (CAPC).⁵⁴ CAPC are similar to BAPC in their ability to self-assemble, however, CAPC can encapsulate hydrophobic compounds, such as oils and hydrophobic dyes.⁵⁴ CAPC are formulated using the peptide Ac-FLIVI-KKKKK-CO-NH₂. Since CAPC can encapsulate hydrophobic compounds, they offer the unique ability to encapsulate and deliver molecules with low aqueous solubility. As with BAPC, CAPC have a simple formulation process allowing for easy assembly of the nano-carriers. One key difference between CAPC and BAPC, are that CAPC are formulated using linear peptide sequences, while BAPC are formulated using branched peptide sequences. While BAPC can self-assemble in water, CAPC require formation in hydrophobic solvents or oils and are sonicated to stabilize suspension of the capsules in aqueous solutions. The ability of CAPC to develop in hydrophobic solvents or oils

allows for them to encapsulate hydrophobic compounds that may have poor cellular uptake due to their hydrophobicity.⁵⁵ But, CAPC allows for more efficient delivery of hydrophobic compounds through encapsulating them. CAPC are stable at high temperatures, up to 90°C, and for over a year when stored at room temperature (22°C) in the dark.⁵⁴ CAPC can facilitate delivery of hydrophobic dyes, such as Nile Red, and hydrophobic oils, such as cannabidiol oil.⁵⁴

Aqueous Partitioning Capsules

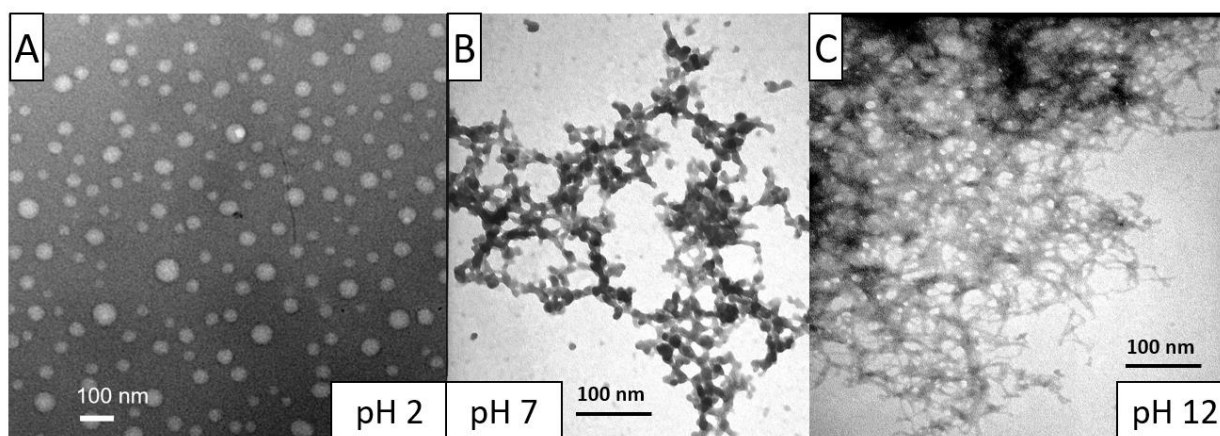


Figure 1.2. $K_3h_5nK_3$ peptide forms nanospheres at pH 2, different structures at higher pH. Transmission electron microscopy (TEM) images of $K_3h_5nK_3$ peptide taken at A) pH 2 (imaged at 34,000x) B) pH 7 imaged at 70,000x and C) pH 12 (imaged at 70,000x). Images were produced using a Hitachi STEM 4800 EM (Hitachi High Tech Group, Germany). Peptides are labeled with methyl mercury on their C-terminal. A droplet (20 μ l) of each sample was placed onto a 200-mesh Formvar-coated grid. Samples were dried at 55°C in a drying oven for 30 min before visualization. Scale bar is 100 nm. Reproduced from Barros, et al.¹⁴

Another novel example of peptide-based nano-carriers are Aqueous Partitioning Capsules (APC). The first description of the peptides that compose APC were in a paper from Mo et. al.⁵⁶, which characterized the peptide Ac-KKKFLIVIKKK-COHN₂ ($K_3h_5nK_3$) and explored it for use as an adhesive. In this publication, the researchers showed that $K_3h_5nK_3$ was a strong adhesive at a pH of 12.⁵⁶ Multiple peptides were analyzed during this study, but the sequence KKK-FLIVI-KKK was among the strongest adhesives.⁵⁶ The dry adhesion strength was tested by using the peptide to glue two pieces of wood planks together and applying shear pressure until the bond broke.⁵⁶ The APC peptide exhibited a dry adhesion strength of 3.27 ± 0.19 MPa.⁵⁶ Wet adhesion

strength was determined through measuring the pressure at which the bond would fail after adhering two pieces of wet wood together. The wet adhesion strength was less, being a shear pressure of 1.13 ± 0.25 MPa.⁵⁶

Along with exploring the adhesive properties of the peptide, secondary structure was characterized using circular dichroism (CD). The CD spectra obtained at a basic pH of 12 revealed it formed β -sheet secondary structures.⁵⁶ Other sequences, studied in Mo et al., that did not show strong adhesion strength did not form β -sheets at basic pH. This suggests that the presence of β -sheet secondary structures are needed to improve the assembly properties. During exploration of the adhesive properties of the $K_3h_5nK_3$ peptide, transmission electron microscopy (TEM) images were taken at pH of 2, 7, and 12, as shown in **Figure 1.1**.¹⁴ The TEM images revealed that at pH of 2, APC formed small nanospheres. At pH 12 TEM images showing the peptides having formed intertwined nanofibrils. Nanofibril intertwining at basic pH may be an explanation for the strong adhesive properties. At pH 7, the peptides form random coil secondary structures. At pH 7, the same adhesive properties seen at pH 12 are not exhibited. The formation of nanospheres at a pH 2, as opposed to the nanofibrils seen at pH 7, is intriguing as the protonation status of lysine differs little over this pH range, as the amino group has a pKa of approximately 9 and the side chain has a pKa of approximately 10.5.

Based solely on the TEM images, it is not clear whether the peptides at a pH of 2 are forming solid or hollow capsules. Therefore, I explored the possibility of using the KKK-FLIVI-KKK peptide as a peptide-based nanocarrier, like BAPC and CAPC. This work explores the dye, mRNA, and plasmid encapsulation and delivery abilities of APC. Variations of the peptide sequence Ac-KKK-FLIVI-KKK-CO-NH₂ ($K_3h_5nK_3$) were examined, including Ac-KKK-IVILF-KKK-CO-NH₂ ($K_3h_5K_3$) and Ac-KKK-FLIVIGSII-KKK-CO-NH₂ ($K_3h_9K_3$). **Table 1.1** shows

the sequences explored during this project along with their molecular masses. Encapsulation of genetic materials and aqueous dyes within APC was explored. Attachment of genetic materials to the outside of APC were explored, due to the large number of lysine residues in the primary sequence, which contain a positive charge at both acidic and neutral pH. The negatively charged genetic material is proposed to attach to these positively charged lysine residues.

Peptides	Sequence	MW (g/mol)
K₃h_{5n}K₃	KKK-FLIVI-KKK	1378.1
K₃h₉K₃	KKK-FLIVIGSII-KKK	1742.3
K₃h₅K₃	KKK-IVILF-KKK	1378.1

Table 1.1. APC peptide sequences. Peptide amino acid sequences used to formulate APC, along with their molecular masses.

Chapter 2 - Characteristics of APC

Materials and Methods

Peptide Synthesis

Solid phase peptide synthesis was used to generate the peptides that form APC. Peptides were synthesized on either a PS3 peptide synthesizer (Protein Technologies inc.; Tucson, AZ) or a CS Bio CS136X peptide synthesizer (CS Bio; Silicon Valley, CA). These systems employ different methods to synthesize the peptides, but both employ Fmoc amino acids that were obtained from BioSystems, Inc. (Windsor, CO).

Amino acid synthesis on the PS3 peptide synthesizer was performed on a 0.5 mmol scale. Each cartridge was loaded with 0.5 mmol of the desired amino acid, 0.068 grams of 1-Hydroxy-7-azabenzotriazole (HOAt) (AAPPTec, Louisville, KY) and 0.190 grams of 1-[Bis(dimethylamino)methylene]-1H-1,2,3-triazolo[4,5-b]pyridinium 3-oxid hexafluorophosphate (HATU) (P3 Biosystems, Louisville, KY) were added. Peptide synthesis was completed while under Nitrogen gas. The reagents used for peptide synthesis on the PS3 peptide synthesizer included dimethylformamide (DMF), 20% piperidine, and 0.4 M N-methylmorpholine (NMP) (Thermo Fisher Scientific, Waltham, MA). CLEAR-Amide Resin, 100-200 mesh and 0.3-0.5 meq/g, was employed (Biosynth, Staad, Switzerland). Peptide synthesizers were attached to two nitrogen gas cylinders, with the primary cylinder having a pressure set at 80 pounds per square inch (PSI) and the secondary cylinder having a pressure of 70 PSI. Once the reaction vesicle was secured to the synthesizer, the solvent bottles and lines were pressurized and primed. The correct sequence of peptides to be synthesized was programmed into the peptide synthesizer. The primary sequences were KKK-FLIVI-KKK, KKK-IVILF-KKK, or KKK-FLIVIGSII-KKK (**Table 1.1**). Reaction vesicle washes used 4 mL DMF with a consistent time of 5 min and amino

acid washes used 500 μ l with a consistent time of 5 min. After the reaction was completed, the resin was dried using a vacuum and dichloromethane (DCM). The resin was weighed, and the peptide was prepped for either capping or cleavage.

When preparing amino acids for peptide synthesis on the CS Bio peptide synthesizer, they were prepared in 4-5 molar excess of amino acids versus resin, per coupling. Amino acids were dissolved in 15 mL of DMF per the number of couplings. HOAt was prepared at 0.4 M in 15 mL of DMF, multiplied by the number of couplings. HATU was prepared at 0.2 M in 30 mL of DMF, multiplied by the number of couplings. The peptides were synthesized onto clear amide resin and peptide synthesis was accomplished under nitrogen gas. The reagents used for synthesis included 50% DMF/50% NMP, DCM, acetyl capping cocktail (for capping), 0.2 M HATU in DMF, 0.4 M HOAt in DMF, 0.8 M N,N-Diisopropylethylamine in DMF, and 20% piperidine in DMF. The correct amino acid sequence for the peptide synthesis was programmed into the CS Bio program. The primary sequences used are shown in **Table 1.1** and include KKK-FLIVI-KKK, KKK-IVILF-KKK, or KKK-FLIVIGSII-KKK. The filter in the reaction vesicle was then replaced and the reaction vesicle was added onto the peptide synthesizer. The resin was added to the reaction vesicle, using DCM to wash any remaining resin into the reaction vesicle. Peptide synthesis was then allowed to begin. Once the peptide synthesis was completed, the resin was dried using vacuum suction and DCM. The resin was then weighed and prepped for cleavage.

The peptides were next cleaved from the resin at room temperature for 90 min, using 92% trifluoroacetic acid (TFA), 5% thioanisole, 2% 1,2-ethanedithiol, and 1% distilled, deionized water. Filtration was then done to remove any excess liquids. To precipitate the peptide, ice cold diethyl ether was used. Three more consecutive washes using diethyl ether were

done to precipitate the peptide. The peptides were lyophilized through suspension in deionized water. Peptides were dried using vacuum and stored as a solid at room temperature in 50 mL Falcon tubes.

Preparation of APC

The dried peptides were dissolved in purely 2,2,2-trifluoroethanol (TFE) after synthesis and cleavage. The concentration of the peptide solution was determined by measuring the absorbance of phenylalanine at a wavelength of 257.5 nm, on a CARY 50 Bio UV-visible spectrometer (Agilent Technologies, Santa Clara, CA). The concentration of peptide in solution was then calculated using Beer's Law ($A = \epsilon c l$ ($A =$ absorbance, $\epsilon =$ molar extinction coefficient, $c =$ concentration, $l =$ path length):

$$A = \epsilon c l$$

The path length was 0.3 cm, as absorbance measurements were taken using a 0.3 cm length quartz cuvette. The molar extinction coefficient of phenylalanine at 257.5 nm, which is $195 \text{ M}^{-1} \text{ cm}^{-1}$, was used for calculations. Concentrations were adjusted to 1 mM in TFE, unless indicated otherwise. Solvent was removed using a vacuum evaporation and APC were rehydrated with a buffer of specified pH. APC were rehydrated for characterization with buffers at pH 2 10 mM glycine-HCl, pH 7 10 mM imidazole, adjusted with HCl, and pH 12 sodium hydroxide (NaOH). Sodium acetate/acetic acid (10 mM) buffers were used for the pH range 3.00-4.56. If specified, APC were formed at acidic pH, they incubated at room temperature for 1-20 min before increasing the pH to 7, through addition of imidazole-HCl buffer. pH for buffers was confirmed using an Orion 2 Star pH benchtop probe (Thermo Fisher Scientific, Waltham, MA). The Orion 2 Star pH benchtop probe was calibrated using pH 4.00 Buffer Solution Red,

pH 7.00 Buffer Solution Yellow, and pH 10.00 Buffer Solution Blue prior to measurements (Avantor, Radnor, PA).

Preparation of mRNA- or dsDNA-APC's nanoparticles

For encapsulation of the genetic material within APC, 200 ng of the genetic material was added to 20 μ l of pH 2 glycine-hydrochloric acid (HCl) buffer. The 20 μ l of pH 2 buffer with the genetic material was immediately used to rehydrate the APC. APC were then allowed to incubate at room temperature for 1-20 min before increasing the pH to 7 using 80 μ l of 10 mM imidazole buffer. Imidazole buffer was prepared at a concentration of 10 mM and pH was adjusted to 7 using HCl. For attachment of the genetic material to the outside of APC, 20 μ l of the pH 2 glycine-HCl buffer was used to rehydrate the APC. APC were allowed to incubate for 5 min at room temperature in the pH 2 buffer, before adding 200 ng of genetic material. After adding the genetic material, APC were allowed to incubate at room temperature for 1-20 min, before increasing the pH to 7 using 80 μ l of 10 mM imidazole buffer. The APC were then used immediately for transfections or for characterization studies after being formulated. pH for samples was confirmed using pH 0-14 indicator paper (Cytvia, Buckinghamshire, United Kingdom).

Circular dichroism

CD spectral data were collected using a Jasco-815 spectrophotometer (Jasco Analytical Instruments, Easton, MD). Samples were prepared as previously described in **Preparation of APC**. Samples were prepared at a range of pH including pH 2, pH 7, pH 12, and in TFE. The buffer used for pH 2 was 10 mM glycine-HCl buffer. The buffer used for pH 7 was 10 mM imidazole buffer, which was adjusted to a pH of 7 using HCl. NaOH was used for samples at pH 12. While running samples, nitrogen gas from a cylinder was allowed to flow through the CD

spectrophotometer. The type of cuvette used to collect data was a 1 mm path length quartz cuvette (Starna Cells Inc., Atascadero, CA). The wavelength range scanned was 260 nm to 190 nm, using 50 nm/min as the scan rate. 1 nm step intervals were used during the scans. A total of five scans were recorded and averaged for each sample. Ellipticity was measured using millidegrees as the units. A Savitsky-Golay filter was used to smooth the spectrum; this analysis of the data was provided for by the manufacturing company. Data was corrected based on the solvent used, in the CD measurements, either TFE, water, or buffers were used as solvents. The type of solvent used depended on the pH of the sample or chemical solvent used to rehydrate the APC.

Dynamic light scattering and zeta potential characterization

APC were prepared at a concentration of 1 mM as previously described (**Preparation of APC and Preparation of mRNA- or dsDNA-APC's nanoparticles**). The particle sizes and zeta potentials for each of the samples was analyzed using a Zetasizer Nano ZS (Malvern Instruments Ltd, Westborough, MA). The particle size measurements were completed using a quartz cuvette to hold the sample. The temperature of the Zetasizer was set to 25°C. A total of 25 runs were completed by the Zetasizer during each measurement, giving standard deviations along with the particle sizes. The results given after each measurement included size distribution profiles and polydispersity. Based on the diffusion coefficient (D), the particle size with the greatest number of particles in the solution was recorded. Sizes are calculated based on the following Stokes-Einstein equation (k [Boltzmann's constant] = 1.381×10^{-23} J/K, T = absolute temperature, n = viscosity, D = diffusion coefficient):

$$d_H = \frac{kT}{3\pi nD}$$

Calculations are completed automatically using proprietary software (Zetasizer). For Zeta potential measurements were conducted in quartz (Omega) cuvettes at 25°C, with power adjusted to a maximum of 200 V. Three-hundred and forty measurements were made on each sample and the mean Zeta potential was reported.

Nanoparticle Tracking Analysis

Nanoparticle tracking analysis (NTA) was performed using a NanoSight LM 14 (Malvern Panalytical, UK). A single chamber was connected to a 405 nm laser and digital images were acquired (Hamamatsu Photonics K. K. CMOS camera Model # C11440-50B). The samples were injected into the single chamber using sterile syringes (BD Discardit II, New Jersey, USA). Videos were acquired at 25.0 frames per second over a period of 60 seconds. The temperature was kept consistent at 25.0 °C. APC capsules were prepared at a concentration of 1 mg/mL as previously described in **Preparation of APC**, at either pH 2 or pH 3. The buffer used for pH 2 was 10 mM glycine-HCl buffer and the buffer used for pH 3 was 10 mM acetic acid/sodium acetate buffer. Images were analyzed to calculate number and size of APC nanoparticles in solution (NanoSight NTA 3.3).

Results and Discussion

Circular Dichroism

CD was used to determine the secondary structures of peptides in solution. Random coils, α -helices, and β -sheets each exhibit distinctive CD spectrums. Random coil CD spectra are characterized by drop in CD (mDeg) around 200 nm which subsequently increases and levels out through a wavelength of 260 nm.^{57,58} α -helical CD spectra are characterized by a tall peak of CD (mDeg) at 190 nm that decreases at approximately 200 and 220 nm.^{57,58} β -sheet CD spectra are characterized by a small peak of CD (mDeg) at approximately 200 nm, with a decrease around 210 nm.^{57,58}

Circular dichroism was used to determine the secondary structure of the $K_3h_{5n}K_3$ peptides that compose APC at different pH values, with results shown in **Figure 2.1**. The pH used were the same as in the original TEM images (**Figure 1.2.**); pH 2, pH 7, and pH 12. At pH 2, $K_3h_{5n}K_3$ peptides appear to form random coil secondary structures, showing a distinctive minimum in CD (mDeg) near 200 nm. APC formulated at pH 7 also exhibit a distinctive minimum in CD (mDeg) at 200 nm characteristic of random coil secondary structure. At pH 12, $K_3h_{5n}K_3$ peptides are shown to form β -sheets, with a peak in CD spectra at approximately 200 nm and a dip in CD spectra at approximately 220 nm. The $K_3h_{5n}K_3$ peptides forming β -sheets confirms the observations in Mo et al., which revealed the same information about the secondary structure at basic pH. Interestingly, when APC are initially formed at a pH of 2, but then increased to a pH of

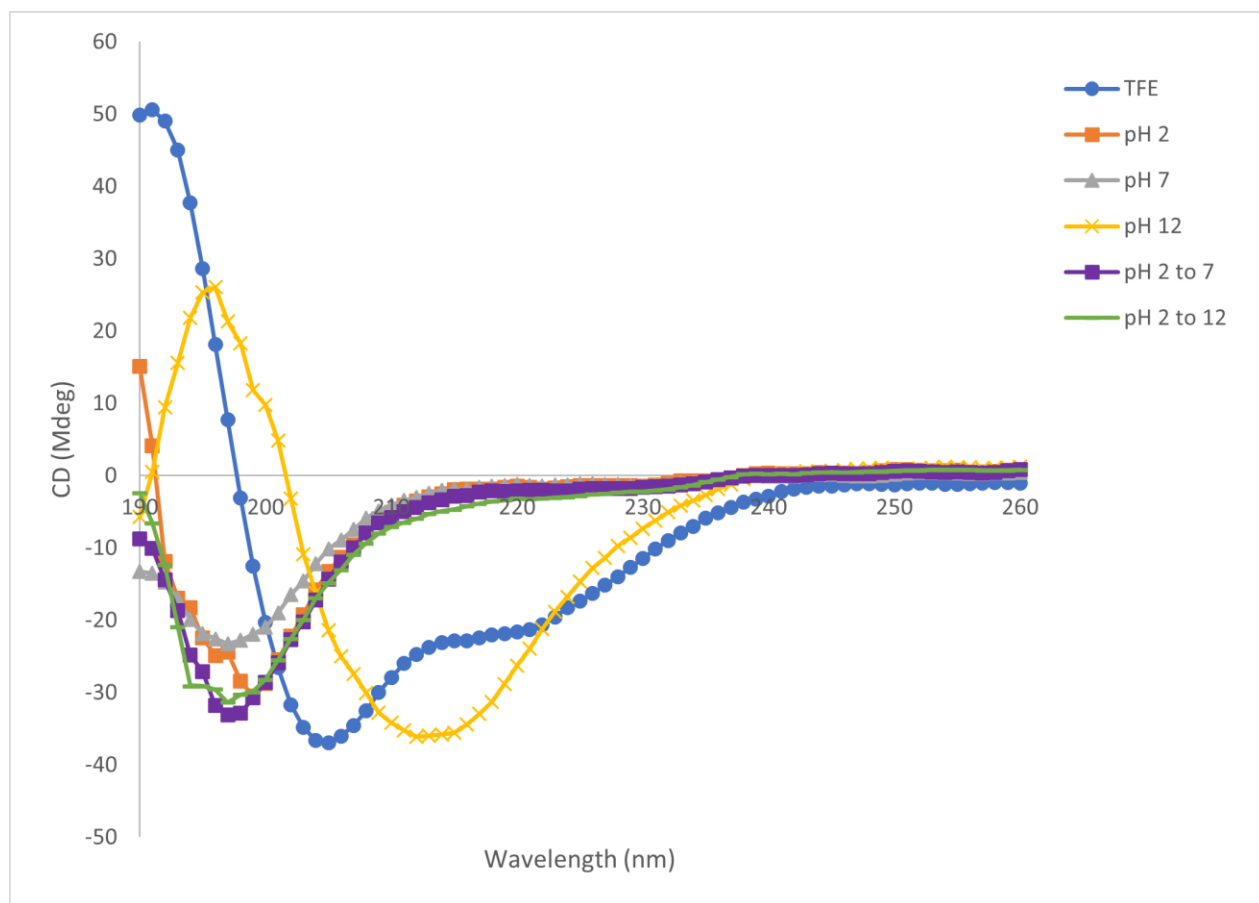


Figure 2.1. $K_{3h_{5n}}K_3$ peptide forms random coils at acidic and neutral pH, β -sheets at basic pH. Circular dichroism data for APC ($K_{3h_{5n}}K_3$) at different pH values and in TFE. Samples were formulated at 1 mM concentration in TFE (1385 mM, pH 7) (represented by blue line, circles), pH 2 10 mM glycine-HCl buffer (represented by orange, squares), pH 7 10 mM imidazole buffer (represented by gray line, triangles), pH 12 NaOH solution (represented by yellow, crosses), initially at pH 2 10 mM glycine-HCl buffer but increased to pH 7 using imidazole buffer after 5 min (represented by purple line, squares), and initially at pH 2 10 mM glycine-HCl buffer but increased to pH 7 using pH 12 NaOH solution (represented by green lines, line). Horizontal axis represents wavelength in nanometers and the vertical axis represents CD measurement in mdeg. Each line represents the average of three runs ($n=3$).

12, a β -sheet conformations are not induced. Rather, the secondary structures of these APC are shown to remain as a random coil. This observation indicates that once formed at an acidic pH, the secondary structure becomes stable and resistant to further changes in pH. In TFE, $K_{3h_{5n}}K_3$ peptides are shown to form an α -helical secondary structure, exhibiting a peak at 190 nm that decreases at approximately 200 and 220 nm. In TFE, $K_{3h_{5n}}K_3$ peptides remain as individual α -helical peptides, as opposed to formulating APC.

α -helices are typically monomeric in nature, meaning that capsules, including APC, cannot properly form when the peptides constituting them have secondary structures that are α -helical. Therefore, looking into at which concentration of TFE α -helices begin to form, can be useful since it could determine at which concentration capsules would begin to break open. This could help allow for quantification of contents of capsules, since forcing capsules to break open and release contents could be done by adding TFE.

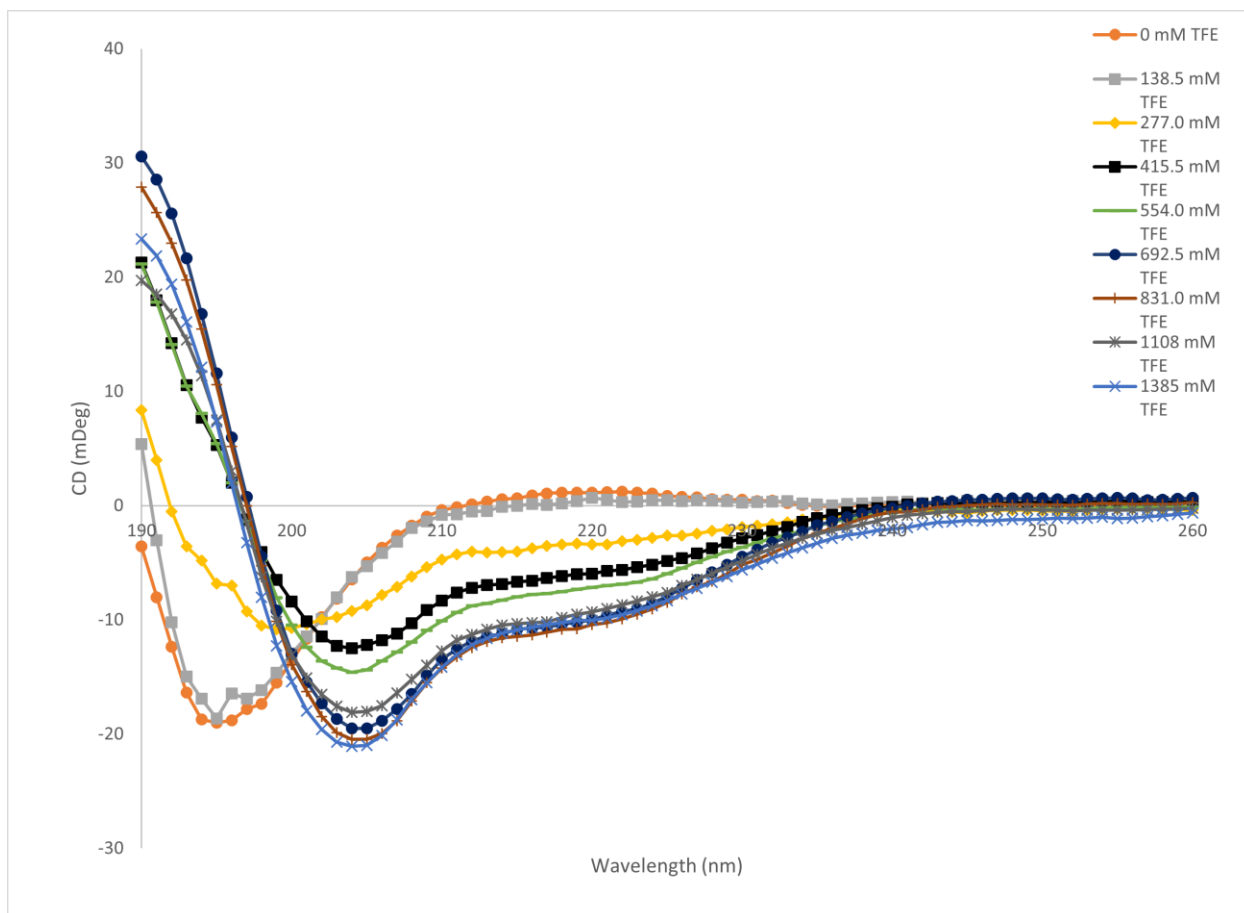


Figure 2.2. TFE induces secondary structure change in $K_3h_5nK_3$ peptides from random coils to α -helices. Circular dichroism spectra for APC peptides ($K_3h_5nK_3$) in increasing concentrations of TFE, ranging from 0 mM to 1385 mM. TFE concentrations used were 0 mM (represented by orange line, circles), 138.5 mM TFE (represented by gray line, squares), 277.0 mM TFE (represented by yellow line, diamonds), 415.5 mM TFE (represented by black line, squares), 554.0 mM TFE (represented by green line, lines), 692.5 mM TFE (represented by navy line, circles), 831.0 mM TFE (represented by red line, crosses), 1108 mM TFE (represented by dark gray line, asterisk), 1385 mM TFE (represented by blue line, x's) and Horizontal axis represents wavelength in nanometers and the vertical axis represents CD measurement in mdeg. Each line represents the average of three samples ($n=3$).

Due to the results in **Figure 2.1** showing $K_{3h_{5n}}K_3$ peptides to form α -helices in TFE, CD was again employed to study the stability of $K_{3h_{5n}}K_3$ peptides in TFE. Increasing concentrations of TFE were used to explore at which concentration $K_{3h_{5n}}K_3$ peptides secondary structures reorganized from random coils to α -helices. $K_{3h_{5n}}K_3$ peptides were exposed to increasing concentrations of TFE, ranging from 0 mM (0%) to 1385 mM (100%) TFE, as shown in **Figure 2.2**. $K_{3h_{5n}}K_3$ peptides consistently form random coils, having CD spectra with a dip around 200 nm that flattens out through 260 nm, from 0-277.0 mM (0-20%) TFE (**Figure 2.2**). All concentrations at or above 415.5 mM (30%) TFE show α -helical secondary structure, exhibiting peaks at 190 nm with minima at 200 nm and 220 nm. Disruption of the random coil secondary structure through TFE, a hydrophobic solvent, suggests that APC may assemble using hydrophobic interactions.

CD spectra were also obtained from the $K_{3h_9}K_3$ peptide; KKK-FLIVIGSII-KKK. This sequence, like $K_{3h_{5n}}K_3$, exhibited a random coil secondary structure at pH 2, pH 3.5 and pH 7 (**Figure 2.3A.**). Along with analyzing $K_{3h_9}K_3$ peptides on CD, $K_{3h_5}K_3$ peptides were also analyzed using CD (**Figure 2.3B.**). The results for the CD spectra of $K_{3h_{5n}}K_3$ peptides also random coil secondary structures at acidic and neutral pH. Addition of four hydrophobic amino acid residues (GSII), for the $K_{3h_9}K_3$ peptides, does not disrupt the secondary structure observed in the $K_{3h_{5n}}K_3$ peptide. Reversal of the hydrophobic interior from FLIVI ($K_{3h_{5n}}K_3$) to IVILF ($K_{3h_5}K_3$) also does not alter the secondary structure. These results suggest the importance of the flanking KKK segments on both C- and N-terminals are important in secondary structure formation. With the hydrophobic interior segments playing a role in secondary structure

formation as well, but mainly due to their hydrophobicity, as opposed to their specific order within the primary sequence.

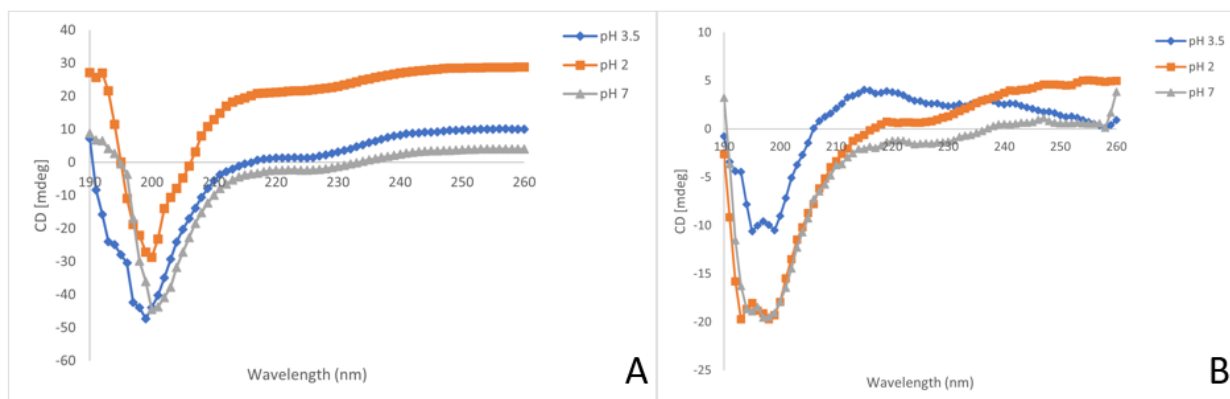


Figure 2.3. $K_{3h5}K_3$ and $K_{3h9}K_3$ peptide forms random coils at acidic and neutral pH. Shown are the CD spectra for the $K_{3h5}K_3$ and $K_{3h9}K_3$ peptides that also compose APC, taken at different pH. Panel A) CD spectra for $K_{3h9}K_3$ taken at pH 2 (represented by orange line, squares), pH 3.5 (represented by blue line, diamonds) and pH 7 (represented by gray line, triangles). Panel B) CD spectra for $K_{3h5}K_3$ taken at pH 2 (represented by orange line, squares), pH 3.5 (represented by blue line, diamonds) and pH 7 (represented by gray line, triangles). Horizontal axis represents wavelength measurement in nanometers and vertical axis represents CD measurement in mdeg.

Dynamic Light Scattering

Sample	Size (nm)	Polydispersity	Zeta Potential (mV)
TFE	686.6 ± 209	34.0%	n/a
pH = 2.00	155.8 ± 33	20.7%	6.4
pH = 7.00	243.5 ± 57	29.2%	1.2
pH = 12.0	2047.5 ± 1283	29.0%	-3.9
pH = 2.00 to 7.00	175.6 ± 100	26.1%	9.3
pH = 2.00 to 12.0	3015 ± 2148	28.0%	-0.6

Table 2.1. DLS shows APC sizes increase as pH is increased. Dynamic light scattering analysis of APC at different pH and in TFE (1385 mM). Sizes shown with standard deviation and $n = 3$.

DLS was used to determine size and polydispersity; to characterize the size and variation among the individual APC in solution.^{59,60} The Zetasizer used to complete the DLS measurements, can also measure Zeta potential. On DLS, APC were analyzed at various pH, as in the original TEM images (**Figure 1.1**), measurements were taken at pH 2, pH 7, and pH 12,

shown in **Table 2.1**. Along with these pH values, APC were analyzed in TFE. These DLS results suggest that APC form smaller particles, approximately 100-200 nm, when formed at highly acidic pH, with size increases as pH is raised. In TFE, pH 7, and pH 12, APC have sizes too large to be considered as possible nano-carriers. Their large size would cause difficulties in passing through cellular membranes, making them less ideal for delivering drugs or genetic materials. The large size seen in APC formed at pH 12 is expected, based on the TEM images (**Figure 1.2.**) that revealed formation of nanofibrils at basic pH. APC formulated at neutral and basic pH exhibit both larger particle and a broader range of particle sizes. The smaller size of APC at pH 2 make them a candidate for being a delivery system. The positive surface charge of the particles is another quality making APC a possible delivery system, as particles with a positively charged surface are more likely to penetrate cell membranes than particles with negatively charged surfaces.^{40,61} A highly positive surface charge also allows for the possibility of attaching negatively charged molecules to the surface of the capsules. Interestingly, when APC are formed at a pH 2 but, have the pH increased to 7 shortly after formation, the size remains like APC formed and kept at pH 2. The Zeta potential also remains positive, being +9.3 mV, when the APC are formed at pH 2 and then have the pH raised to pH 7. These results, along with corresponding CD spectra, indicate that forming APC at a pH 2 before increasing to pH 7, allows APC formulation in the strongly acidic pH and maintaining their formulation through transition to neutral pH.

pH 5 min → pH 7	Size (nm)	Polydispersity	Zeta Potential (mV)
2.00	85.4 ± 67	17.7%	14.3
2.49	62 ± 52	31.2%	8.2
3.00	84.8 ± 27	28.4%	15.9
3.30	71.8 ± 34	29.0%	10.8
3.51	92.5 ± 85	24.7%	5.9
3.90	151 ± 93	27.8%	10.5
4.56	187.8 ± 166	29.4%	7.5

Table 2.2. APC form nanosized particles when formed at pH of 3.51 and below (5-minute incubation). Characteristics of APC at different pH values and with an incubation time of 5 min before increasing the pH to 7, obtained using DLS. Size shown with standard deviation and n = 3.

Next, APC were formulated using various acidic pH, to determine the maximum pH that could be employed to produce nano-sized particles. Genetic material, in particular mRNA, is notoriously unstable. Therefore, examining characteristics of APC formation over a range of acidic pH could reveal that APC may form nanocapsules at a pH higher than 2, which would be more optimal for mRNA. APC were formed at an acidic pH, ranging from 2.00-4.56, and allowed to incubate at the acidic pH for either 5 min or 20 min before increasing the pH to neutral. For the 5-minute incubation at acidic pH, APC formed particles ranging from 50-100 nm in size, with an increase in size seen at 3.90 and above resulting in 200-300 nm sized particles (**Table 2.2.**). For the 20-minute incubation at acidic pH, APC formed particles ranging from 100-200 nm in size, with an increase in size seen at 3.51 and above resulting in 200-500 nm sized particles (**Table 2.3.**). The sizes seen with the longer incubation time (20-min) were overall larger than those with short incubation times (5-min). One consistency throughout both **Tables 2.1.** and **2.2.** is that Zeta potentials remain highly positive throughout the entire acidic pH range. These results show that APC surface charge remains cationic throughout the pH range of 2.00-4.56.

pH 20 min → pH 7	Size (nm)	Polydispersity	Zeta Potential (mV)
2.00	135.2 ± 12.4	27.90%	14.4
2.49	193.1 ± 140.6	23.90%	7.70
3.00	192.7 ± 149	24.10%	8.30
3.30	140.5 ± 69.8	29.90%	7.00
3.51	239.8 ± 189	34.90%	11.6
3.90	207.5 ± 87.7	33.90%	5.50
4.56	493 ± 320	24.80%	8.50

Table 2.3. APC form nanosized particles when formed at pH of 3.51 and below (20-minute incubation). Characteristics of APC at different pH values and with an incubation time of 20 min before increasing the pH to 7, obtained using DLS. Sizes shown with standard deviation and n = 3.

APC created using the K₃h₅K₃ peptide were also analyzed on DLS, formulated at either pH 2, pH 3.9, pH 7, or pH 12, shown in **Table 2.4**. The results for K₃h₅K₃ APC were like those seen in K₃h_{5n}K₃ APC (**Table 2.1**). These results suggest that creating APC with either K₃h_{5n}K₃ or K₃h₅K₃ exhibit similar size characteristics. Sizes of K₃h₅K₃ APC when formed at a pH 2 were 143.2 nm and the zeta potential was +5.7 mV, both like the results of the forward APC sequence formed at pH 2 (**Table 2.1**). The Zeta potential decreases from 5.7 mV, at pH 2, to -6.8 mV as pH is increased to 12. However, one difference in size characteristic data of K₃h₅K₃ APC is a greater increase in the standard deviation of all pH tested. This suggests that the size distribution of APC created using K₃h₅K₃ peptides is much greater than exhibited in K₃h_{5n}K₃ APC. One explanation for this observation is that the inversion of hydrophobic interior amino acids from FLIVI (K₃h_{5n}K₃) to IVILF (K₃h₅K₃) causes a disruption in particle formation, resulting in increased range of size distribution of APC. Zeta potential increases as pH increases, a trend seen in APC formulated from K₃h_{5n}K₃ (**Table 2.1**).

pH	Size (nm)	Polydispersity	Zeta Potential (mV)
2.00	143.2 ± 210	33.00%	5.7
3.90	282 ± 191	38.30%	0.7
7.00	191.3 ± 160	35.20%	-0.2
12.0	2479 ± 1419	33.80%	-6.8

Table 2.4. APC formulated from K₃h₅K₃ peptides exhibit similar trends in particle size as APC formulated from K₃h_{5n}K₃ peptides. Characteristics of inverted APC sequence, formed at pH 2, 3.90, 7.00, and 12.0. Sizes shown with standard deviation and n = 3.

These results reveal that 1-minute and 5-minute incubation times for this sequence give particles between the range of 100-300 nm. The 20-minute incubation time yields particles with a smaller particle size of 38 nm. While the 1-minute and 5-minute incubation times reveal formation 100-300 nm size particles. This suggests that along with forming larger particles, there is also a greater size range of particles when formed at a 20-minute incubation time.

Neutralization Time (min)	Size (nm)	Polydispersity
1	148.0 ± 97	29.7%
5	264.0 ± 100.4	37.5%
20	38.0 ± 12	30.1%

Table 2.5. APC formulated from K₃h₉K₃ peptides exhibit similar trends in particle size as APC formulated from K₃h_{5n}K₃ peptides. Characteristics of extended APC sequence, formed at pH 3.50. Sizes shown with standard deviation and n = 3.

Nanoparticle Tracking Analysis

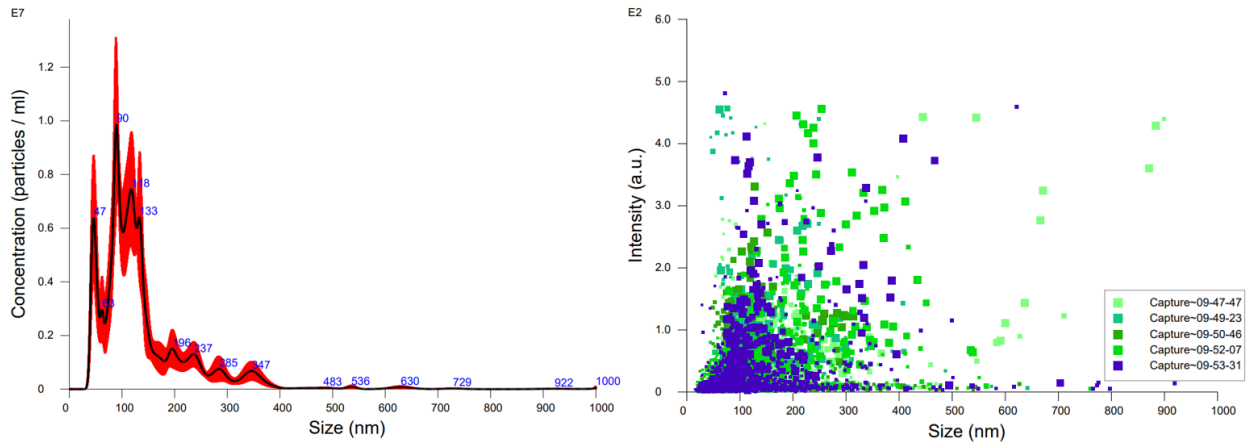


Figure 2.4. NTA reveals size distribution profile of APC formulated at pH 2, showing particle size between 100-200 nm. Panel A) Size distribution of particles in solution. Vertical axis represents concentrations of particles per mL and horizontal axis represents particle size in nm. B) Intensity of the sizes of particles in solution. Vertical axis represents intensity (a.u.) and horizontal axis represents size in nm.

Along with DLS, NTA was also used to characterize the size of the particles in solution. NTA is a technique that employs use of a video camera to visualize and record each individual particle in solution using a laser and ultramicroscope.⁶² This technique allows for the measurement of each individual particle in solution, compared to DLS which measures a size distribution profile of the particles in solution.^{59,62} Usage of NTA allows for visualization of individual particles in solution through video taken during measurements.^{62,63} Employing both DLS and NTA to measure the size of the particles can help ensure the accuracy of the size characterization of APC in solution.

NTA analysis of APC formed at pH 2 showed a mean size of 139.1 nm, with a standard deviation of 8.9 nm, and a mode size of 94.7 nm, with a standard deviation of 13.1 nm. These results are consistent with the data obtained from DLS, in which sizes were 100-200 nm (**Table 2.1**). The size distribution profiles of all particles in solution, for APC formulated at pH 2, are shown in **Figure 2.4**. The size distribution profiles obtained using NTA allow for a complete

profile and better assessment of particle sizes in solution, showing that majority of particles are about 100 nm, with very few particles above 200 nm.

NTA analysis of APC formed at pH 3 showed a mean size of 240.1 nm, with a standard error of 104.0 nm, and a mode size of 230.9 nm, with a standard deviation of 104.6 nm. These results are also consistent with data obtained on DLS, which showed sizes of 200-300 nm when APC were formulated at a pH of 3 (Tables 2.3-2.4). The size distribution profiles of these APC, formulated at pH 3, in solution are shown in Figure 2.5. The size distribution profiles obtained using NTA allow for a better look into the sizes of each individual particle in solution, showing that most particles are about 200 nm. Unlike APC formed at pH 2, the APC formulated at pH 3 have many more particles above the size of 300 nm, with some particles above the size of 1000 nm. The results of NTA confirm that APC formulate smaller nanocapsules when formed at a pH of 2, as opposed to being formulated at a pH of 3. NTA results suggest that APC formulated at pH 2 exhibit both smaller particle sizes and lower particle size distribution than APC formulated at pH 3.

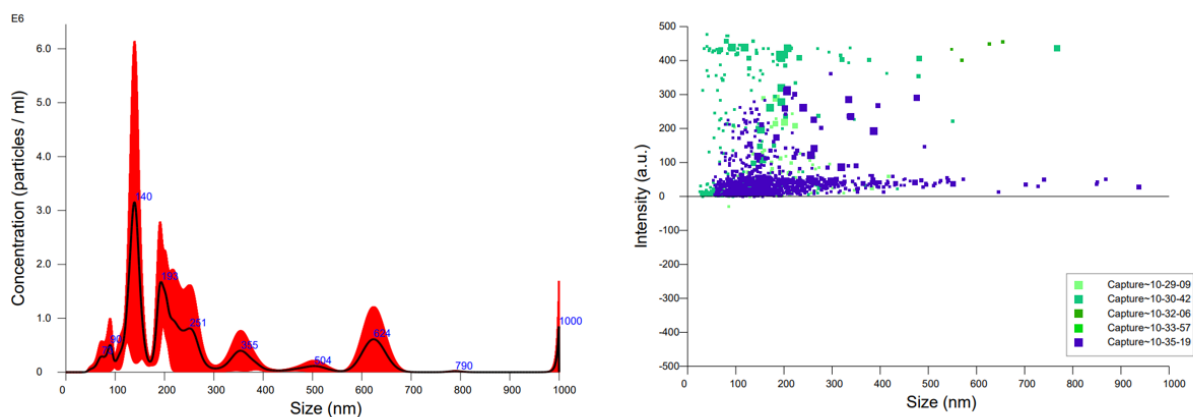


Figure 2.5. NTA reveals size distribution profile of APC formulated at pH 3, showing particle size between 200-700 nm. Panel A) Size distribution of particles in solution. Vertical axis represents concentrations of particles per mL and horizontal axis represents particle size in nm. B) Intensity of the sizes of particles in solution. Vertical axis represents intensity (a.u.) and horizontal axis represents size in nm.

Discussion

The use of CD, DLS, and NTA allowed for insight into the size and secondary structure characteristics of APC. CD spectral data revealed that secondary structure of all peptide sequences, KKK-FLIVI-KKK, KKK-FLIVIGSII-KKK, and KKK-IVILF-KKK, all form random coil secondary structures when formed at both acidic and neutral pH. The use of a hydrophobic solvent, TFE, to disrupt the random coil secondary structure into an α -helices suggests hydrophobic interactions play a major role in formation of nanocapsules. DLS and NTA reveal particle size increases as pH is increased, with the smallest particles forming at pH 2 and the largest aggregates forming at pH 12. However, when APC are initially formed at pH 2, but later have their pH increased to 7, the particle size does not increase drastically. Rather, the size of these particles remains comparable to particles made and kept at pH 2. This same trend is observed in CD spectra, where forming the APC initially at pH 2, but increasing the pH to 12, does not induce the β -sheet secondary structure. Instead, the secondary structure remains a random coil. These trends suggest that once initially formed at pH 2, raising the pH will not alter the size and secondary structure characteristics. Although use of these techniques is important in determining the potential viability in using APC as a genetic material or drug delivery system, the next step will be to use APC to deliver genetic materials or water-soluble dyes into cell lines. Delivery of genetic materials and dyes to mammalian cells lines would indicate that APC can encapsulate solutes, entering cells, and releasing their contents into the cells.

Chapter 3 - Delivery and Encapsulation of Genetic Materials and

Dyes Using APC

Materials and Methods

APC dye encapsulation

APC were prepared as previously described in **Preparation of APC**. Rhodamine 6G was added to 1.0 mL of pH 2, 10 mM glycine-HCl buffer, giving a final dye concentration of 100 μ M. Rhodamine 6G dye in glycine-HCl buffer was used to rehydrate APC. Samples were placed into Amicon Ultra centrifuge filters, with a molecular weight cut-off of 30 kDa (EMD Millipore, Billerica, MA). Samples were washed with water three times and spun at 3000 RCF for 3 min at 25°C using a Prism R Refrigerated Microcentrifuge tabletop (Labnet, Edison, NJ). Samples were washed a fourth time with 200 μ L of 200 mM sodium trifluoroacetic acid (TFA) at 3000 RCF for 3 min at 25°C. Centrifuge filters were then inverted into clean tubes and spun once more at 3000 RCF for 1 min at 25°C, to remove the APC containing dye. Samples of APC with encapsulated rhodamine 6G dye were placed onto a glass slide and allowed to dry at room temperature (25°C). Once completely dried, the slides were analyzed using a confocal LSM 700 laser-scanning microscope (Carl Zeiss, Gottingen, Germany). An excitation wavelength of 350 nm was used to visualize the dye.⁶⁴ Images taken on the confocal microscope were analyzed using ZEN 3.5 (blue edition).

APC GFP plasmid and GFP mRNA transfections

Human embryonic kidney (HEK) and baby hamster kidney (BHK) cells were grown at 37°C with 5% CO₂. HEK and BHK cells were grown in 4.5 g/L glucose Dulbecco's Modified Eagle medium with penicillin-streptomycin and fetal bovine serum (Corning, Inc., Corning, NY). Media was replaced every 72 hours. Cells were seeded into Thermo Scientific Lab-Tek II CC2 8 well cell trays, at a concentration of 2.5×10^4 cell per well to prepare for transfections. Cells grew until reaching a confluence of at least 70% before transfections were conducted.

APC were prepared for transfection as previously described in **Preparation of mRNA- or dsDNA-APC's nanoparticles**. Different ratios of APC to genetic material were tested during transfections, along with testing both attachment to the surfaces and encapsulation within APC. Different ratios of genetic material to APC peptide tested included 1:5 (w/w), 1:10 (w/w) and 1:20 (w/w). Ratios always included 200 ng of either green fluorescence protein (GFP) plasmid or mRNA (TriLink Biotechnologies, San Diego, CA). The amount of peptide was 1 µg in the 1:5 ratios, 2 µg in the 1:10 ratios, and 4 µg in the 1:20 ratios. The exact volume of APC used was calculated based on obtaining the concentration of stock solution of APC, as described previously in **Preparation of APC**, and using the molecular masses of the peptides (**Table 1.1**) to determine the volume required to obtain the desired mass of APC. The volume of genetic material was calculated by obtaining the concentration of the genetic material on a NanoDrop, ND-1000 Spectrophotometer to determine the volume needed to get 200 ng of GFP plasmid or GFP mRNA (Marshall Scientific, Hampton, NH).

HEK and BHK cell media were refreshed immediately before transfection with Opti-MEM Reduced Serum (Thermo Fisher Scientific, Waltham, MA). APC were sterilized using ultraviolet light for 30 min, immediately before transfections. Designated conditions were added

to individual wells, immediately after formulation of the mRNA- or plasmid DNA-APC. Cells were exposed to GFP-containing APC for 44 hours. Cells were fixed using 4% perfluoroalkoxy alkanes (PFA) in phosphate buffered saline (PBS), at pH 7.4. After termination of transfections and fixing of cells, media was replaced with PBS (American Type Culture Collection, Manassas, VA). Cell membranes were permeabilized with 0.1% Triton X for 1 hour (Thermo Fisher Scientific, Waltham, MA). After permeabilization of the cell membranes, the cells were washed with PBS. The cell tray was then allowed to completely dry before adding SlowFade™ Diamond Antifade Mountant with 4',6'-diamidino-2-phenylindole (DAPI), to stain the nuclei of the cells (Thermo Fisher Scientific, Waltham, MA). A 25 x 55 mm glass coverslip was placed on top of the cell tray and sealed using clear nail polish (Thermo Fisher Scientific, Waltham, MA). The cell tray was covered in aluminum foil and stored at room temperature before analyzing on a confocal microscope. Images were taken using a LSM 700 laser-scanning microscope (Carl Zeiss, Gottingen, Germany). The images taken on the confocal microscope were analyzed using ZEN 3.5 (blue edition).

For analysis of the transfections on the Countess II FL cell counter, HEK cells were grown in 36-well plate (Life Technologies, Rockville, MD). Cells were dissociated from the plate using 50 µl of 0.8% trypsin. Cells incubated for 2 min in trypsin, before removing 10 µl of cells to place into a microcentrifuge tube. To stain for cell viability, 20 µl of trypan blue solution was added. Cells (10 µl) were removed and placed into Countess™ cell counting chamber slides and subsequently analyzed on the Countess™ II FL cell counter for cell viability and GFP fluorescence (Invitrogen, Waltham, MA).

RiboGreen Assays

RiboGreen™ assays were completed in 96-well plates. Samples for testing were prepared as described previously in **Preparation of mRNA- or dsDNA-APC's nanoparticles**.

Immediately after sample preparation, APC were dispensed into 96-well plates. Each well included 0.5 µl of Quant-iT™ RiboGreen™ reagent in 100 µl of 1X Tris/EDTA (TE) buffer (Thermo Fisher Scientific, Waltham, MA). Each condition under analysis was made in a triplicate. After adding RiboGreen™ reagent to each well, the 96-well plate was immediately covered with aluminum foil and taken to a plate reader for analysis. The fluorescence was measured with an excitation wavelength of 480 nm and an emission wavelength of 520 nm.^{65,66}

Gel Electrophoresis

APC samples were prepared with GFP plasmid both encapsulated and surface-bound, as described previously in **Preparation of mRNA- or dsDNA-APC's nanoparticles**. After APC formation and incubation with GFP plasmid, they were allowed to digest for 30 min at 37°C with DNase I, from bovine pancreas grade II (Roche Diagnostics GmbH, Mannheim, Germany). Once samples were done digesting, 5 µl of TE buffer and 50 µl of 1X orange DNA loading dye were added to samples. Gels were made with 0.8% agarose and contained ethidium bromide to visualize DNA. MOPS was used as the running buffer for the gels. Samples were resolved for 50 min at a consistent 100 V. Once the gels were done running, MOPS running buffer was drained from the chamber and gels were removed from the chamber. Gel images were acquired using a gel viewer.

Nanoparticle Tracking Analysis

NTA was performed using a NanoSight LM 14 (Malvern Panalytical, UK), as described previously in Chapter 2 **Nanoparticle Tracking Analysis**. Samples were prepared as described previously in **Preparation of mRNA- or dsDNA-APC's nanoparticles**. APC were prepared at a ratio of 1:10 (w/w) for genetic material to peptide. Poly I.C. was used to prepare samples (Sigma-Aldrich, Saint Louis, MO). The amount of poly I.C. was kept consistent at 200 ng and 2 μ g of APC peptide were used. Samples were analyzed immediately after preparation.

Results and Discussion

Encapsulation of Rhodamine 6G Dye

Before looking into possible delivery capabilities of APC, encapsulation of solutes dissolved in water was first analyzed. APC were formulated at pH 2 in a solution of rhodamine 6G dye. The APC were subsequently washed using sodium TFA, placed onto a glass slide, allowed to dry, and analyzed on confocal microscopy. Encapsulation of rhodamine 6G dye was confirmed using confocal microscopy, as shown in **Figure 3.1**. APC can be seen with encapsulated rhodamine 6G dye, confirming that the nano-capsules that form at pH 2 are capable of encapsulating both aqueous solvents and solutes. However, one drawback to analyzing APC using confocal microscopy is that there is a limit to the size of particles able to be viewed. The

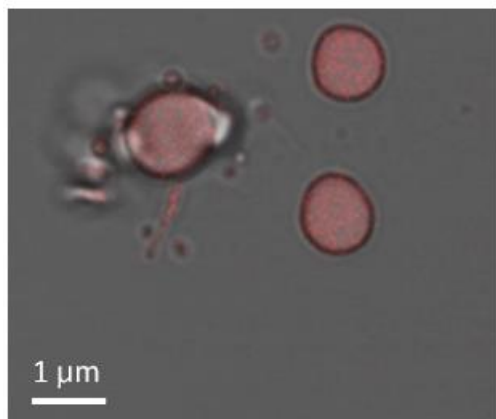


Figure 3.1. APC encapsulates rhodamine 6G dye. Confocal microscopy of APC encapsulating the fluorescent dye-rhodamine 6G. APC are roughly 1-2 microns in diameter, as anything smaller than 1-2 microns will be undetectable by the confocal microscope. Scale bar shown represents 1 μm.

detection limit for the confocal microscope is 1-2 microns, therefore, any particles smaller than this will be undetectable. This detection limit is much larger than the particle sizes previously obtained using DLS and NTA, therefore APC with encapsulated rhodamine 6G in **Figure 3.1** represent APC of a much larger size than most capsules described in the previous chapter. However, the confocal images still reveal pertinent information, including confirmation of encapsulated rhodamine 6G dye and support of capsule formation.

GFP Plasmid Transfections Using APC

Following encapsulation of a water-soluble dye, APC were analyzed for their ability to encapsulate genetic materials, as well as bind the genetic materials to the surface of the capsules, and subsequently deliver the genetic material into cells. HEK cells were transfected with GFP plasmid using APC as the transfection agent; with GFP plasmid either encapsulated within APC or surface bound. The negative control shown in images is HEK cells only, with no transfection reagent used (**Figure 3.2A.**). Lipofectamine 3000™ is an example of a cationic lipid-based transfection reagent that is marketed commercially. Lipofectamine 3000™ complexes with negatively charged genetic materials to deliver across cell membranes.³⁷ As previously mentioned, liposomes self-assemble in aqueous solutions by forming a lipid bilayer with a cationic surface. The negatively charged genetic materials then complex with the cationic surface charge on the liposomes. Lipofectamine 3000™ transfection reagent is designed specifically to deliver DNA and dsRNA to cells. Lipofectamine 3000™ is efficient at delivery of plasmids to cells, however, is not typically used in any clinically applications, due to its high cytotoxicity.^{37,67} Even with its high cytotoxicity, Lipofectamine 3000™ is a useful tool in research settings to deliver DNA to cells, and therefore, is a useful comparison when assessing the transfection ability of APC (**Figure 3.2B.**).

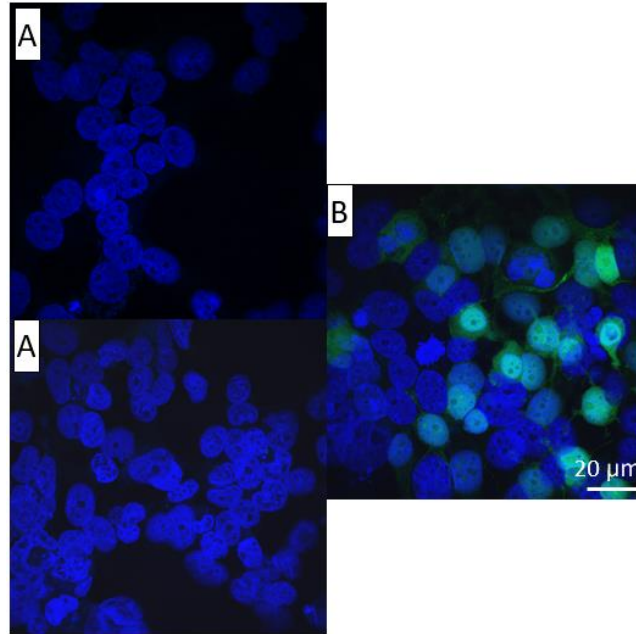


Figure 3.2. Human embryonic kidney cells treated with either no transfection reagent or Lipofectamine 3000™ complexed with GFP plasmid. All nuclei are stained blue with DAPI. Green stain is GFP fluorescence. Panel A) HEK cells treated with no transfection reagent. Panel B) HEK cells treated with Lipofectamine 3000™ complexed together with 200 ng of GFP plasmid. Scale bar shown represents 20 μm.

APC with surface bound GFP plasmid showed successful transfection of the DNA into HEK cells (**Figure 3.3.**). HEK cells treated with APC complexed surface bound GFP plasmid show expression of GFP, indicating APC have penetrated cell membranes and delivered the plasmid (**Figure 3.3.**). The w/w ratio of GFP plasmid to APC peptide with the most efficient transfection was 1:10, which showed the greatest amount and intensity of GFP fluorescence (**Figure 3.3B.**). These confocal images show that APC, when prepared at a ratio of 1:10 GFP plasmid to peptide, exhibit stronger expression of GFP in HEK cells than Lipofectamine 3000™ (**Figure 3.2B.**).

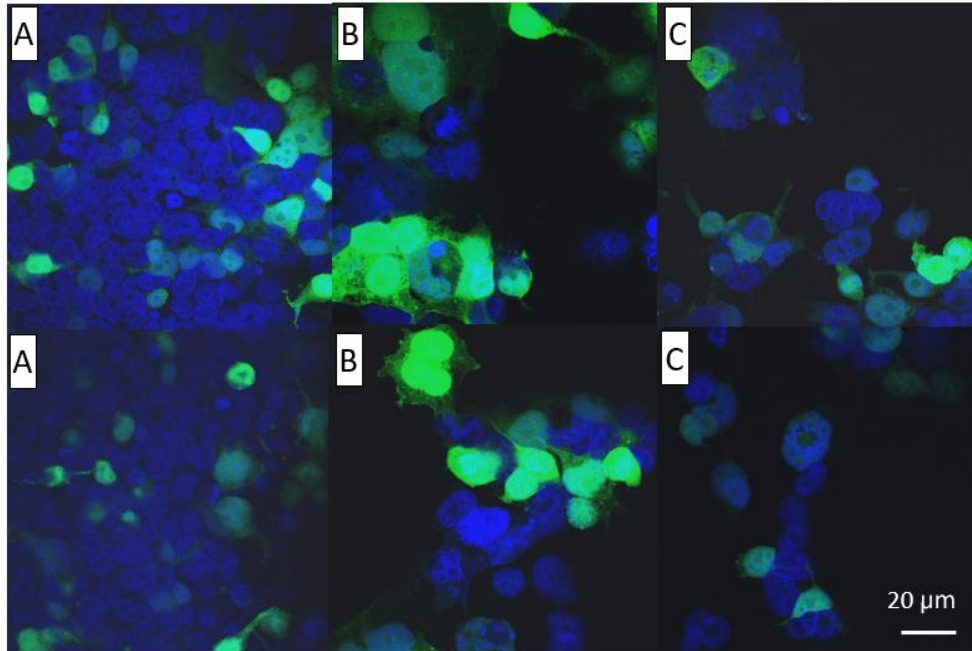


Figure 3.3. APC deliver surface bound GFP plasmid to HEK cells. All nuclei are stained blue with DAPI. Green stain is GFP fluorescence. Panel A) HEK cells treated with APC containing surface bound GFP plasmid (at a w/w ratio of 1:20 GFP plasmid to APC peptide) as the transfection reagent. Panel B) HEK cells treated with APC containing surface bound GFP plasmid (at a w/w ratio of 1:10 GFP plasmid to APC peptide) as the transfection reagent. Panel C) HEK cells treated with APC containing surface bound GFP plasmid (at a w/w ratio of 1:5 GFP plasmid to APC peptide) as the transfection reagent. Scale bar shown represents 20 μm .

In **Figure 3.4**, APC containing encapsulated GFP plasmid showed successful transfection of the DNA into HEK cells. Similarly, to APC complexed with surface bound GFP plasmid, containing encapsulated GFP plasmid were most efficient at gene delivery at a w/w GFP plasmid to APC peptide ratio of 1:10 (**Figure 3.4B.**). Overall, the GFP plasmid transfection using APC as the transfection reagent showed APC could facilitate uptake of GFP plasmid into HEK cells. Compared to Lipofectamine 3000 reagentTM, APC elicit much more intense fluorescence in the HEK cells. These results reveal that at each ratio of GFP plasmid to peptide, 1:5, 1:10 and 1:20, APC are capable penetrating HEK cell membranes and delivery of plasmid. Images also suggest that the 1:10 ratio of genetic material to peptide, of both APC with encapsulated and surface bound GFP plasmid, results in the strongest uptake of plasmid into cells (**Figure 3.3B.** and

Figure 3.4B.). However, it does not reveal whether APC are encapsulating GFP plasmid. Therefore, further studies need to be done to characterize the differences between APC made with intentions of encapsulating GFP plasmid versus attaching GFP plasmid to the surface. Still, these GFP plasmid transfection results reveal APC can penetrate cells membranes to deliver DNA for expression.

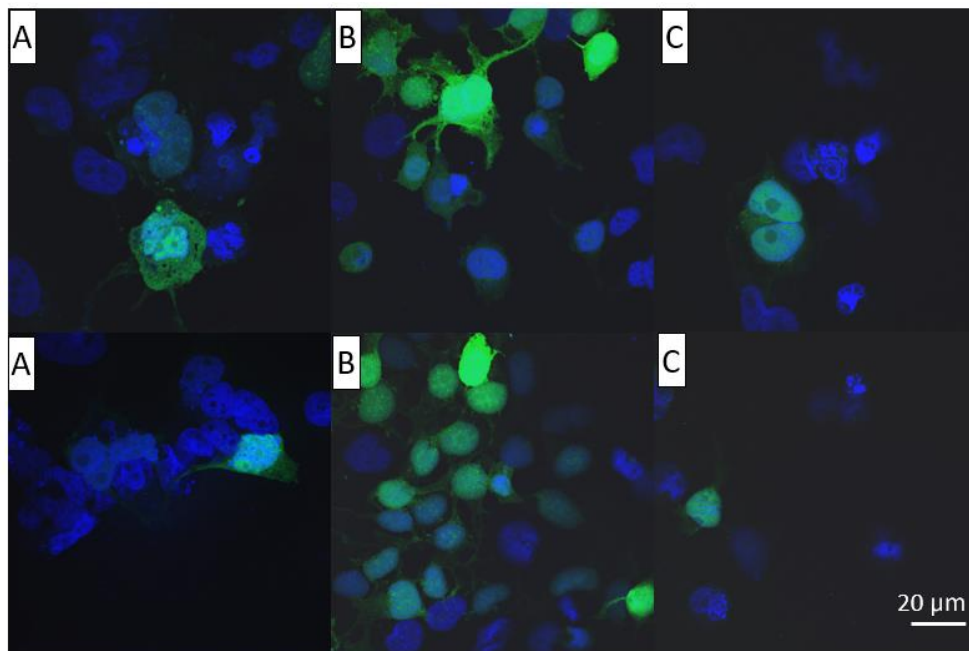


Figure 3.4. APC deliver encapsulated GFP plasmid to HEK cells. All nuclei are stained blue with DAPI. Green stain is GFP fluorescence. Panel A) HEK cells treated with APC containing encapsulated GFP plasmid (at a w/w ratio of 1:20 GFP plasmid to APC peptide) as the transfection reagent. Panel B) HEK cells treated with APC containing encapsulated GFP plasmid (at a w/w ratio of 1:10 GFP plasmid to APC peptide) as the transfection reagent. Panel C) HEK cells treated with APC containing encapsulated GFP plasmid (at a w/w ratio of 1:5 GFP plasmid to APC peptide) as the transfection reagent. Scale bar shown represents 20 μm .

The sizes of APC complexed with GFP plasmid were analyzed on DLS to determine their size and charge characteristics. The sizes of each APC, whether with GFP plasmid encapsulated or attached to the outside, range from 100-300 nm (**Table 3.1**). These results reveal that when complexed with DNA, APC still formulate particles with sizes compatible with entry into cells.

Sample	Size (nm)	Polydispersity	Zeta (mV)
1:20 Outside	307.6 ± 213	24.00%	4.4
1:20 Inside	171.6 ± 110	33.00%	7.8
1:10 Outside	159.7 ± 101	28.20%	1.7
1:10 Inside	170.9 ± 168	28.00%	2.0
1:5 Outside	113.9 ± 77	25.10%	8.2
1:5 Inside	199.4 ± 12	24.87%	4.4

Table 3.1. APC complexed with GFP plasmid form particles between 100-300 nm in size. Size characteristics of the APC used for GFP plasmid transfection. Sizes shown with standard deviation, and n = 3.

GFP mRNA Transfections Using APC

The GFP mRNA transfections were conducted similarly to GFP plasmid transfections previously discussed, with HEK cells being transfected with GFP mRNA using APC as the transfection agent. Again, APC were formulated with GFP mRNA either encapsulated or surface-bound. The negative control is, again, HEK cells treated with no transfection reagent (**Figure 3.5A.**). The positive control was Lipofectamine™ MessengerMAX™, which is a commercially available lipid transfection reagent, optimized for transfections involving mRNA. Like previously mentioned Lipofectamine 3000™, Lipofectamine™ MessengerMAX™ is a cationic lipid transfection reagent, that works by complexing the negatively charged mRNA to the cationic liposomal surface. Lipofectamine™ MessengerMAX™ is also not used clinically due to cytotoxicity concerns, but can be effective at delivering mRNA, small RNAs, and short dsDNA in research settings. Therefore, Lipofectamine™ MessengerMAX™ can serve as a tool of comparison to determine the ability of APC to transfect cell lines using mRNA (**Figure 3.5B.**).

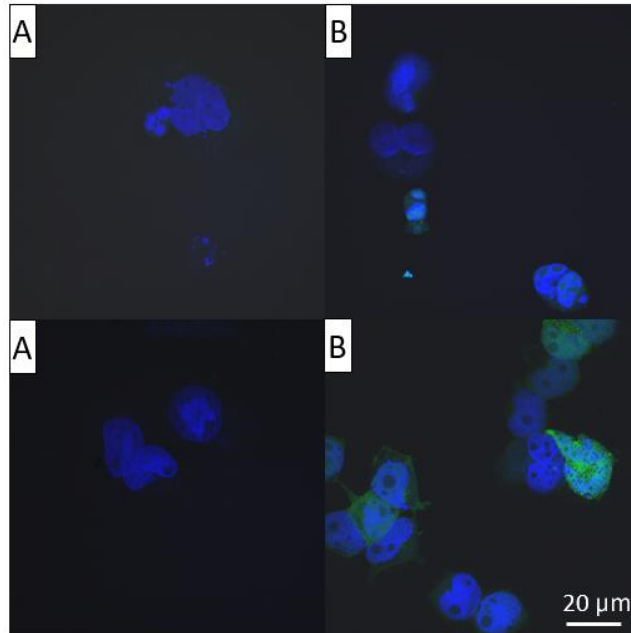


Figure 3.5. Human embryonic kidney cells treated with either no transfection reagent or Lipofectamine MessengerMAX™ complexed with GFP mRNA. All nuclei are stained blue with DAPI. Green stain is GFP fluorescence. Panel A) HEK cells treated with no transfection reagent. Panel B) HEK cells treated with Lipofectamine MessengerMAX™ complexed together with 200 ng of GFP mRNA. Scale bar shown represents 20 μm.

APC with surface bound GFP mRNA showed successful transfection of the mRNA into HEK cells, as cell can be seen expressing GFP fluorescence (**Figure 3.6.**). HEK cells treated with APC complexed surface bound GFP mRNA show expression of GFP, indicating APC have penetrated cell membranes and delivered the mRNA (**Figure 3.6.**). The w/w ratio of GFP mRNA to APC peptide with the most efficient transfection was 1:5, which showed the greatest amount and intensity of GFP fluorescence (**Figure 3.6C.**). Overall, these results show that APC can deliver surface bound GFP mRNA, as GFP fluorescence can be seen in the HEK cells.

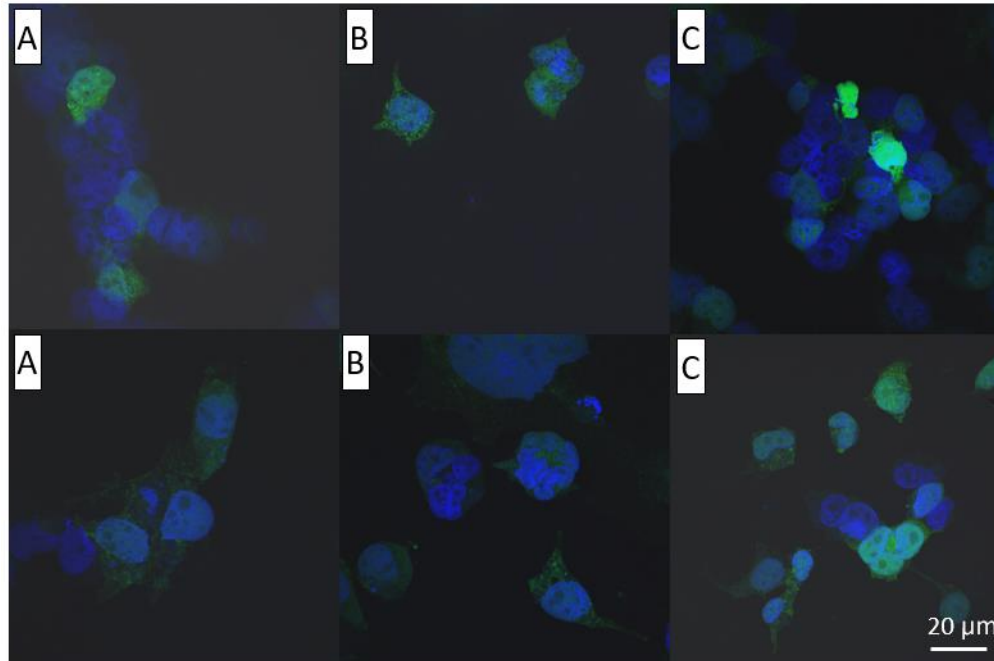


Figure 3.6. APC deliver surface bound GFP mRNA to HEK cells. All nuclei are stained blue with DAPI. Green stain is GFP fluorescence. Panel A) HEK cells treated with APC containing surface bound GFP mRNA (at a w/w ratio of 1:20 GFP mRNA to APC peptide) as the transfection reagent. Panel B) HEK cells treated with APC containing surface bound GFP mRNA (at a w/w ratio of 1:10 GFP mRNA to APC peptide) as the transfection reagent. Panel C) HEK cells treated with APC containing surface bound GFP mRNA (at a w/w ratio of 1:5 GFP mRNA to APC peptide) as the transfection reagent. Scale bar shown represents 20 μm .

These results are similar to those seen in GFP plasmid transfections, with both GFP mRNA and plasmid transfections revealing the w/w ratio of genetic material (either mRNA or plasmid) to APC peptide with most efficient delivery being 1:10. These confocal images show that APC, when prepared at a ratio of 1:10 GFP mRNA to peptide, exhibit stronger expression of GFP in HEK cells than Lipofectamine MessengerMAX™ (**Figure 3.4B.**). Overall, the results of the GFP mRNA transfection, as analyzed by confocal microscopy, show that APC can facilitate uptake of GFP mRNA into HEK cells. The results of the 1:5 (surface bound GFP mRNA) and 1:10 (encapsulated GFP mRNA) ratio APC showed the greatest expression of GFP mRNA when compared to the other ratios tested and the Lipofectamine MessengerMAX™ (**Figure 3.6.**). Along with showing GFP expression in many of cells treated with APC as the transfection reagent, the cell confluence with the 1:5 encapsulated GFP mRNA (**Figure 3.7**) and 1:10

encapsulated GFP mRNA (**Figure 3.6**), showed higher levels of cell confluence when compared to other conditions tested and the controls of HEK cells only and Lipofectamine MessengerMAX™.

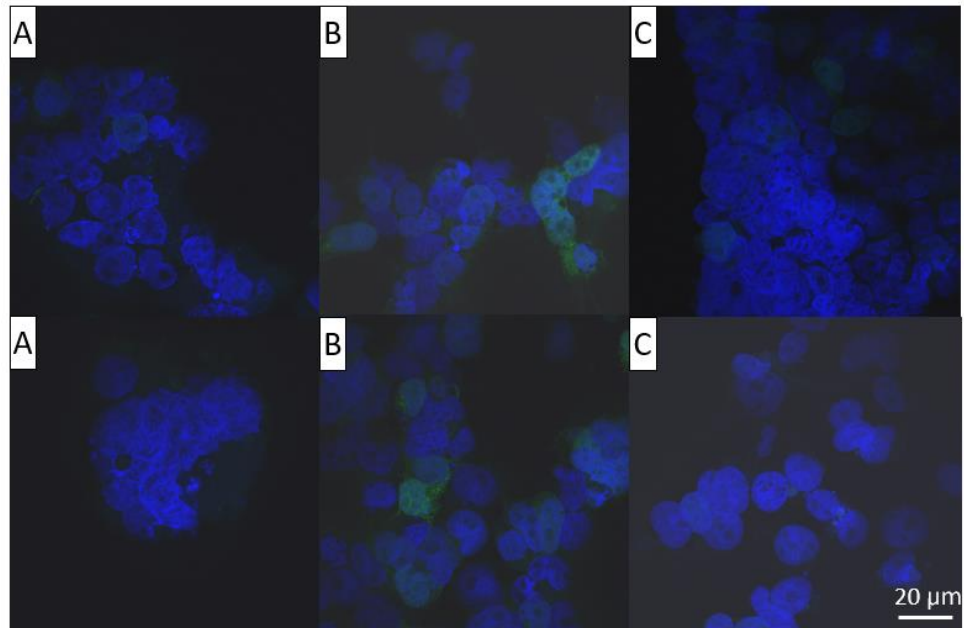


Figure 3.7. APC deliver encapsulated GFP mRNA to HEK cells. All nuclei are stained blue with DAPI. Green stain is GFP fluorescence. Panel A) HEK cells treated with APC containing encapsulated GFP mRNA (at a w/w ratio of 1:20 GFP mRNA to APC peptide) as the transfection reagent. Panel B) HEK cells treated with APC containing encapsulated GFP mRNA (at a w/w ratio of 1:10 GFP mRNA to APC peptide) as the transfection reagent. Panel C) HEK cells treated with APC containing encapsulated GFP mRNA (at a w/w ratio of 1:5 GFP mRNA to APC peptide) as the transfection reagent. Scale bar shown represents 20 μm .

One drawback of confocal microscopy is that it can only give an idea of cytotoxicity, not an exact quantification of cell viability. Therefore, along with analyzing transfected cells using confocal microscopy, a Countess™ cell counter was employed to help validate results seen in confocal microscopy and allow for cytotoxicity assays to be employed. Unlike for the confocal microscopy, with the cell counter, cell viability was able to be calculated using trypan blue staining. Trypan blue penetrates membranes of dead cells, but not living cells. Therefore, cells that become stained with trypan blue are considered nonviable. While cells that do not become stained with trypan blue are considered viable, living cells. Trypan blue (0.4%) solution was used to stain for cell viability during these transfections.⁶⁸ Cells were stained with trypan blue immediately before analysis on the cell counter. Cell viability was automatically calculated on the Countess™, along with total concentration of cells and GFP fluorescence. Cell viability of HEK cells treated with either no transfection reagent or Lipofectamine MessengerMAX™ were determined, as shown in **Figure 3.8**. Cells treated with no transfection reagent have a cell viability of 92%, while cells treated with Lipofectamine MessengerMAX™ have a cell viability of 33%.



Figure 3.8. Cell viability of human embryonic kidney cells treated with no transfection reagent and Lipofectamine MessengerMAX. Panel A) Cell viability of HEK cells treated with no transfection reagent. Cell viability was calculated using 0.4% trypan blue. Trypan blue staining revealed 92% of cells were viable, with 8% of cells dead. Panel B) Cell viability of HEK cells treated with Lipofectamine MessengerMAX (complexed with 200 ng of GFP mRNA). Cell viability was calculated using 0.4% trypan blue. Trypan blue staining revealed 33% of cells were viable, with 67% of cells dead.



Figure 3.9. APC, formulated from $K_3h_{5n}K_3$ peptide, deliver GFP mRNA to HEK cells without affecting cell viability. Panel A) GFP fluorescence of HEK cells treated with APC containing encapsulated GFP mRNA (using a ratio of 1:10 GFP mRNA to $K_3h_{5n}K_3$ peptide) as the transfection reagent. 2% of HEK cells are shown expressing GFP fluorescence. Panel B) Cell viability of HEK cells treated with APC containing encapsulated GFP mRNA (using a ratio of 1:10 GFP mRNA to $K_3h_{5n}K_3$ peptide) as the transfection reagent. Cell viability was calculated using 0.4% trypan blue. Cell viability revealed 88% of cells alive and 12% of cells dead. Panel C) GFP fluorescence of HEK cells treated with APC containing encapsulated GFP mRNA (using a ratio of 1:20 GFP mRNA to $K_3h_{5n}K_3$ peptide) as the transfection reagent. 10% of HEK cells are shown expressing GFP fluorescence. Panel D) Cell viability of HEK cells treated with APC containing encapsulated GFP mRNA (using a ratio of 1:20 GFP mRNA to $K_3h_{5n}K_3$ peptide) as the transfection reagent. Cell viability was calculated using 0.4% trypan blue. Cell viability revealed 86% of cells alive and 14% of cells dead.

HEK cells were treated with either APC, formulated from either $K_3h_{5n}K_3$ peptides or $K_3h_5K_3$ peptides, containing GFP mRNA as the transfection reagents. APC were formulated to encapsulate the GFP mRNA for each of these studies. For APC created using $K_3h_{5n}K_3$ peptides, both GFP mRNA to peptide ratios of 1:10 and 1:20 showed GFP fluorescence, without affecting cell viability (**Figure 3.9**). Cell viability of HEK cells treated with APC remained between 86-88% of cells being viable. These results reveal that APC not only can transfect cells with GFP mRNA but are not negatively affecting cell viability. APC created from $K_3h_5K_3$ peptides also

successfully transfected HEK cells with GFP mRNA, as cells showed GFP fluorescence at both GFP mRNA to peptide ratios of 1:10 and 1:20 (**Figure 3.10.**). Cell viability of these HEK cells remained between 74-82%. Lipofectamine MessengerMAX™ was used as a comparison, again. The cells treated with Lipofectamine MessengerMAX™ did express GFP fluorescence, however, the cell viability was much lower ranging from 33% (**Figure 3.8B.**). Analysis of using APC to deliver GFP mRNA using a cell counter confirmed results previously seen on confocal microscopy, that APC can deliver GFP mRNA into HEK cells. The exact percentage of cells expressing GFP fluorescence could also be calculated automatically using the cell counter. For APC created using K₃h₅nK₃ peptides, 2% and 10% of cells were expressing GFP fluorescence

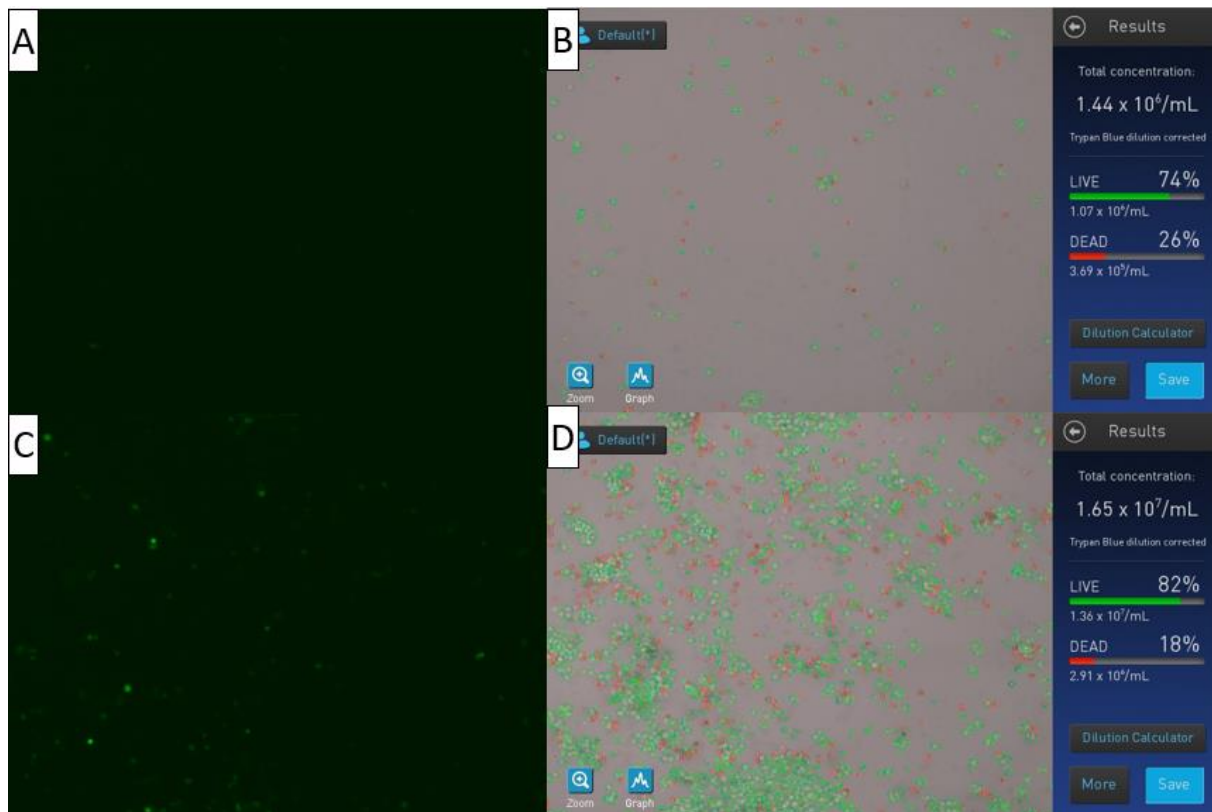


Figure 3.10. APC, formulated from K₃h₅K₃ peptide, deliver GFP mRNA to HEK cells without affecting cell viability. Panel A) GFP fluorescence of HEK cells treated with APC containing encapsulated GFP mRNA (using a ratio of 1:10 GFP mRNA to K₃h₅K₃ peptide) as the transfection reagent. 4% of HEK cells are shown expressing GFP fluorescence. Panel B) Cell viability of HEK cells treated with APC containing encapsulated GFP mRNA (using a ratio of 1:10 GFP mRNA to K₃h₅nK₃ peptide) as the transfection reagent. Cell viability was calculated using 0.4% trypan blue. Cell viability revealed 74% of cells alive and 26% of cells dead. Panel C) GFP fluorescence of HEK cells treated with APC containing encapsulated GFP mRNA (using a ratio of 1:20 GFP mRNA to K₃h₅K₃ peptide) as the transfection reagent. 3% of HEK cells are shown expressing GFP fluorescence. Panel D) Cell viability of HEK cells treated with APC containing encapsulated GFP mRNA (using a ratio of 1:20 GFP mRNA to K₃h₅nK₃ peptide) as the transfection reagent. Cell viability was calculated using 0.4% trypan blue. Cell viability revealed 82% of cells alive and 18% of cells dead.

peptide ratios of 1:10 and 1:20, respectively (**Figure 3.8**). For APC created using $K_{3h_{5n}}K_3$ peptides, 4% and 3% of cells were expressing GFP fluorescence peptide ratios of 1:10 and 1:20, respectively (**Figure 3.9**). Overall, these results suggest that APC are not toxic to HEK cells and confirm the ability of APC to transfect GFP mRNA into cell lines. Since APC are formulated using peptides, these results are consistent with the idea that peptide-based nanoparticles are less toxic than lipid-based nanoparticles or viral vectors.^{14,24,44}

Along with formulating APC using the peptides $K_{3h_{5n}}K_3$ and $K_{3h_5}K_3$ for transfections, $K_{3h_9}K_3$ peptides were used to transfect BHK cells with GFP plasmid and GFP mRNA. $K_{3h_9}K_3$ APC exhibited delivery of both GFP plasmid and GFP mRNA, as shown in **Figure 3.11**. These results suggest that extension of the hydrophobic part of the peptide sequence, from FLIVI to FLIVIGSII, does not interfere with APC ability to deliver genetic materials. This trend supports the idea that small alterations in the hydrophobic segment of the peptides, such as IVILF and FLIVIGSII, do not interfere with the ability of APC to deliver genetic materials.

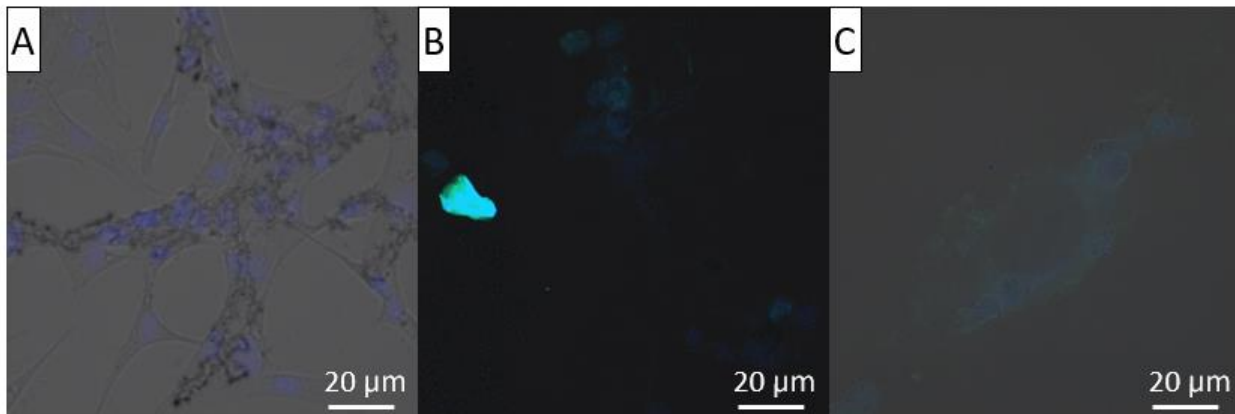


Figure 3.11. APC, formulated from $K_{3h_9}K_3$ peptide, deliver GFP mRNA and GFP plasmid to BHK cells. Confocal images showing BHK cells, with nuclei stained with DAPI and GFP fluorescence. Panel A) BHK cells only. B) BHK cells treated with 1:10 ratio $K_{3h_9}K_3$ APC with GFP mRNA encapsulated as the transfection reagent. C) BHK cells treated with 1:10 ratio $K_{3h_9}K_3$ APC with GFP plasmid encapsulated as the transfection reagent. Scale bar shown represents 20 μ m.

Additional transfections were performed to determine ideal conditions that would facilitate the highest uptake and expression of GFP mRNA in HEK cells. Different incubation times, or the amount of time APC would sit at an acidic pH before raising pH to neutral, were analyzed. APC were formulated with incubation times of 1 minute, 5 min, or 20 min. Along with using a variety of incubation times, different acidic pH values were used. Instead of solely formulating the APC at pH 2, APC were also formulated at pH 3 and pH 3.5. Raising the pH slightly could help reduce damage to the genetic materials that may occur when sitting at the acidic pH for a few min. DLS results shown in **Table 2.1** and **Table 2.2** suggest that APC formed above pH 3.51 begin to aggregate and form larger particles, which would make delivery of genetic materials unlikely.

The results of APC formulated at pH 2, with either 1-minute, 5-min, or 20-min for the incubation time are shown in **Figure 3.11**. These transfections result in GFP expression in the HEK cells, with greatest expression seen in APC formulated with 1-minute and 20-minute incubation times. At both the 1- and 20-minute incubation times almost all HEK cells were expressing some level of fluorescence. The 1-min incubation time showed the highest level of GFP fluorescence compared to all conditions tested, shown in **Figure 3.11C**. One explanation for why this condition revealed high levels of expression is that GFP mRNA only sits at the acidic pH for 1-min, helping to prevent any damage that might occur to the genetic material at acidic pH. APC formed at both pH 3 and pH 3.5 showed either none or very little GFP expression at the 1-, 5-, and 20-min incubation times (data not shown).

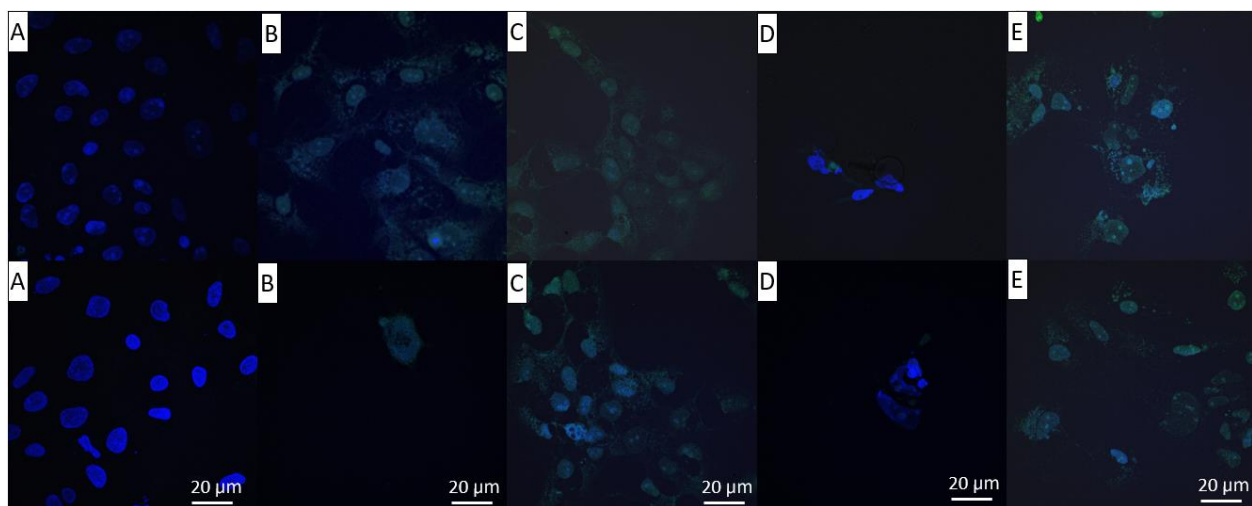


Figure 3.12. APC deliver GFP mRNA to HEK cells. All nuclei stained blue with DAPI. Panel A) HEK cells with no transfection reagent. Panel B) HEK cells treated with 200 ng GFP mRNA and Lipofectamine MessengerMAX™ as the transfection reagent. Panel C) APC (1:10 ratio of GFP mRNA to K₃h₅nK₃ peptide) as the transfection reagent for HEK cells. Peptides rehydrated at pH 2 with 1-min incubation time before increasing pH to 7. GFP mRNA encapsulated within APC. Panel D) APC (1:10 ratio of GFP mRNA to K₃h₅nK₃ peptide) as the transfection reagent for HEK cells. Peptides rehydrated at pH 2 with 5-min incubation time before increasing pH to 7. GFP mRNA encapsulated within APC. Panel E) APC (1:10 ratio of GFP mRNA to K₃h₅nK₃ peptide) as the transfection reagent for HEK cells. Peptides rehydrated at pH 2 with 20-min incubation time before increasing pH to 7. GFP mRNA encapsulated within APC. Scale bars shown represents 20 μm.

These results confirm that APC are most efficient when formed at pH 2, as well as that an incubation time of 1-minute also results in the most efficient delivery of GFP mRNA. Overall results from both transfections analyzed on confocal microscopy and the Countess™ cell counter highlight that APC can deliver mRNA into mammalian cell lines. However, these results do not reveal information about whether APC are encapsulating genetic materials. Since other transfection reagents capable of delivering mRNA to cells work through complexing the negatively charged genetic material to their positively charged surfaces, the idea of encapsulating mRNA within a peptide-based nanoparticle is novel. Damage to genetic material could be limited through encapsulation via APC. Therefore, further experiments need to be conducted to determine if APC are capable of encapsulation of genetic materials, or if they are complexing them to their positively charged surface. Still, these GFP mRNA transfections reveal APC can

protect mRNA from degradation to penetrate cells membranes and deliver mRNA for expression.

RiboGreen Assays

RiboGreen™ assays were employed to determine the differences between APC formulated to encapsulate genetic materials versus those formulated with intentions of complexing genetic material to the surface. The RiboGreen™ reagent fluoresces when exposed to genetic materials, making it a quality assay to assess relative amounts of genetic material present in a given sample.^{65,66} If genetic materials are encapsulated within APC, they would not be available to interact with the RiboGreen™ reagent in the solvent. But genetic material that is surface bound could interact with the RiboGreen™ reagent. Therefore, APC with encapsulated genetic materials should exhibit significantly lower fluorescence than those with surface-bound genetic materials. When using RiboGreen™, samples are excited at a wavelength of 485 nm and emission intensity is measured at a wavelength of 520 nm.⁶⁶ Independent samples student's T test showed that APC with encapsulated poly I.C. (inside samples) and surface-bound poly I.C. (outside samples), at ratios of 10:1 and 1:1, were significantly different; having p-values <0.001 (**Figure 3.13.**). These results suggest that APC are capable of encapsulating genetic materials. However, other ratios tested, including 1:5, 1:10, and 1:20 showed no significant difference between the amount of genetic material detected in the outside versus inside APC (data not shown). One explanation being that when APC are forming around genetic material, they may also have genetic material attached to the outside of capsules after formation. Lower amounts of peptide, 10:1 and 1:1, do show significant differences in relative amounts of genetic material interacting with the RiboGreen™ reagent. Having lower amounts of peptide may help prevent excess genetic material from binding to APC surfaces, as there is less peptide present, and all

peptide present is used for encapsulation. Overall, the results of RiboGreen™ assays reveal there is a difference between APC prepared to encapsulate genetic material versus attach genetic material to the APC surfaces.

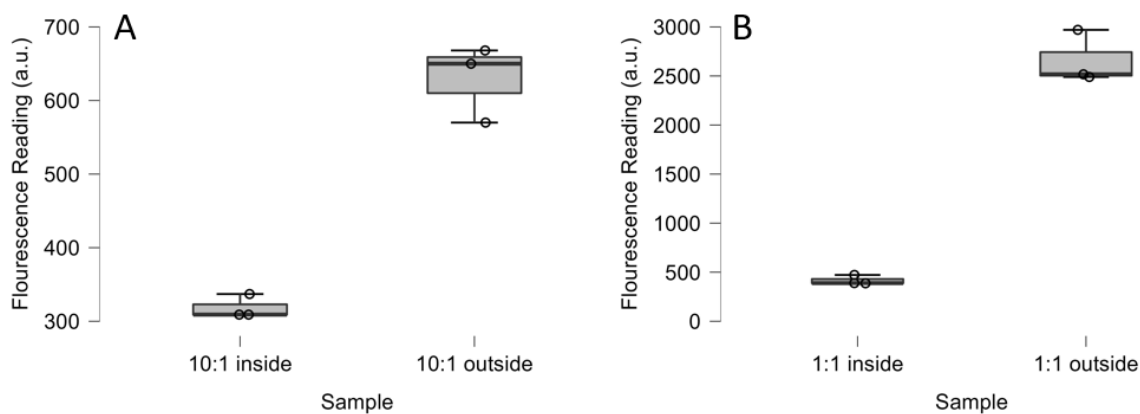


Figure 3.13. RiboGreen assay reveals differences in fluorescence between APC with surface-bound versus encapsulated DNA. Panel A) RiboGreen™ assay results of 10:1 ratio APC, showing comparison between APC with poly I.C. encapsulated versus poly I.C. attached to the outside. Panel B) RiboGreen™ assay results of 1:1 ratio APC, showing comparison between APC with poly I.C. encapsulated versus attached to the outside. The horizontal axis represents the ratio of poly I.C. to $K_3h_{5n}K_3$ peptide tested and the vertical axis represents the fluorescence reading (a.u.).

Gel Electrophoresis

Along with utilizing RiboGreen™ to help determine the location of genetic materials, gel electrophoresis was also used. Digestion of GFP plasmid using DNase was used to study if encapsulation within APC was able to protect DNA from digestion. Controls of GFP plasmid digested and undigested were used to determine the effect of DNase on the genetic material (**Figure 3.14**). GFP plasmid digested with DNase I results in a weaker band expressed than compared to undigested GFP plasmid. In **Figure 3.14.**, lanes 6 and 7 show the 1:1 ratio APC with GFP plasmid encapsulated and attached to the surface, respectively. A weak band can be seen with APC with surface bound GFP plasmid, implying that digestion did occur, and that APC did not protect the DNA. For APC containing encapsulated GFP plasmid, no band can be

seen, showing that APC are protecting the genetic materials. These results support the idea that APC can encapsulate genetic material, as APC formulated for encapsulation confer protection from DNA digestion. Overall, these results indicate that APC with encapsulated plasmid do confer protection against DNase digestion.

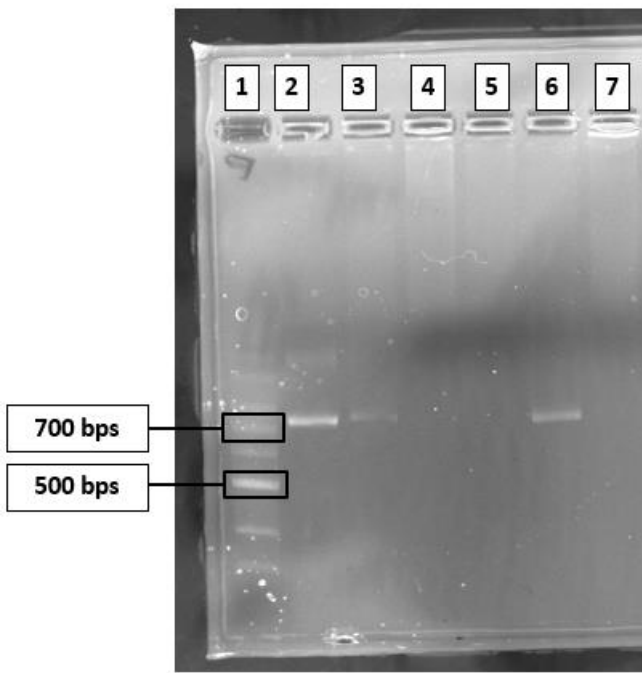


Figure 3.14. APC protects DNA from DNase digestion. Gel electrophoresis performed on APC treated with DNase I for 30 min at 37°C. APC with 200 ng GFP plasmid either encapsulated (inside) or surface-bound (outside). Lane 1) DNA ladder. Lane 2) GFP plasmid (200 ng) with no DNase treatment. Lane 3) GFP plasmid (200 ng) with DNase treatment for 30 min at 37°C. Lane 4) APC with 200 ng GFP plasmid surface-bound (5:1 ratio GFP plasmid to peptide) and treated with DNase. Lane 5) APC with 200 ng GFP plasmid encapsulated (5:1 ratio GFP plasmid to peptide) and treated with DNase. Lane 6) APC with 200 ng GFP plasmid surface-bound (1:1 ratio GFP plasmid to peptide) and treated with DNase. Lane 7) APC with 200 ng GFP plasmid encapsulated (1:1 ratio GFP plasmid to peptide) and treated with DNase.

NTA Characterization of APC with Genetic Materials

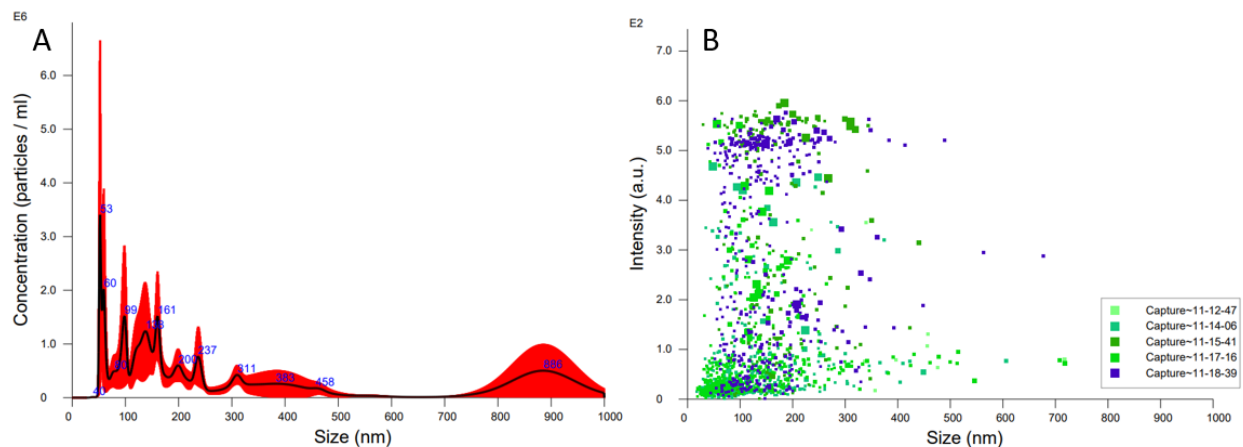


Figure 3.15. NTA reveals size distribution profile of APC with encapsulated DNA forms particles ranging 100-400 nm in size. Panel A) Size distribution of particles in solution. The vertical axis represents concentration of particles per mL and horizontal axis represents particle size measured in nanometers. Panel B) Intensity of the sizes of particles in solution. The vertical axis represents intensity (a.u.) and horizontal axis represents particle size measured in nanometers.

NTA was performed on APC containing poly I.C either surface-bound or encapsulated. NTA results, shown in **Figure 3.15**, revealed that APC with poly I.C. encapsulated had an average size of 270.7 nm, with a standard deviation of 105.9 nm. These results are like those obtained from DLS (**Table 3.1**); that APC with genetic material encapsulated range from 100-300 nm in size. NTA results for APC with surface-bound poly I.C. are shown in **Figure 3.16**. The average size was 246.3 nm, with a standard deviation of 23.1 nm. These results are, again, consistent with results obtained from DLS (**Table 3.1**). Both NTA and DLS size analysis of APC with genetic material surface-bound or encapsulated show the sizes ranging from 100-300 nm in size.

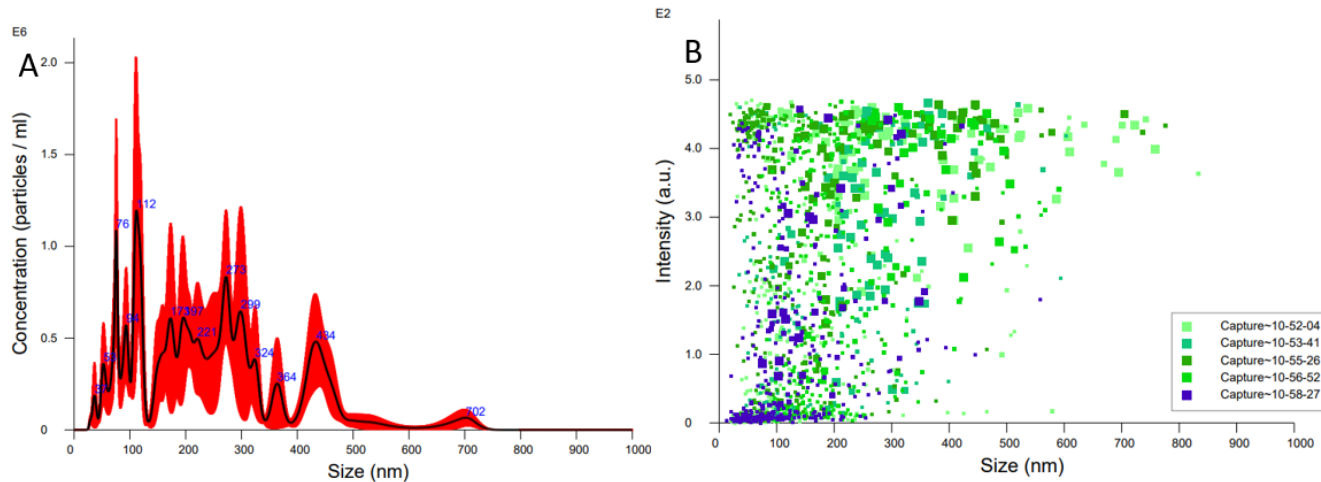


Figure 3.16. NTA reveals size distribution profile of APC with surface-bound DNA forms particles ranging 100-500 nm in size. Panel A) Size distribution of particles in solution. The vertical axis represents concentration of particles per mL and horizontal axis represents particle size measured in nanometers. Panel B) Intensity of the sizes of particles in solution. The vertical axis represents intensity (a.u.) and horizontal axis represents particle size measured in nanometers.

Chapter 4 - Stability of APC

Materials and Methods

Time Stability Studies

The stability of APC over time was assessed by employing DLS/Zeta measurements to track the sizes, polydispersity, and zeta potentials. DLS and Zeta measurements were performed as previously mentioned in **Dynamic light scattering and zeta potential characterization**. One change to the protocol described in this section was that samples stored at 4°C were also assessed at 4°C, to maintain the same temperature throughout the study. Samples stored at room temperature were assessed at 25°C. Samples were stored either on a laboratory benchtop (25°C), while samples stored at 4°C were stored in a refrigerator. All samples were stored in 1.5 mL plastic microcentrifuge tubes. Samples were analyzed on DLS/Zeta to determine their sizes, polydispersity, and Zeta potentials throughout the course of 16-20 days.

Results and Discussion

Time Stability of APC

Since a major factor into the quality of a nano-carrier delivery system is stability, the stability of APC over time was studied through analyzing their size characteristics using DLS.¹⁴ One drawback of delivery vectors that are currently FDA approved that is they are stable only at low temperatures and for short periods.^{8,14,19} Having delivery vectors with stability at higher temperatures and for longer periods would allow for greater access to product on efficiency to use.¹⁴ Using DLS measurements tracked over time can reveal physical stability characteristic of the nanoparticles, as it can assess whether nanoparticles have begun aggregating or degrading.²⁸ Aggregation of APC would impact delivery efficiency, as aggregation would cause increases in particle size that could make APC incompatible with cell penetration. Degradation of APC would impact delivery efficiency, as degradation of particles could result in dissociation with and inability to deliver cargo to cells. Over the course of two weeks to a month, the size of the particles was tracked over time using DLS measurements. To maintain the proper temperature, the DLS Zetasizer was set to measure at either room temperature or 4°C when recording measurements. Both K_{3h_{5n}}K₃ and K_{3h₉}K₃ peptides were tracked for their stability over time.

Day	Size (nm)	Polydispersity	Zeta (mV)
1	88.0 ± 126	27.17%	20.5
2	95.5 ± 138	26.77%	15.7
3	173.7 ± 120	26.47%	6.0
4	131.0 ± 158	28.47%	27.0
5	141.2 ± 122	22.97%	25.0
9	133.9 ± 118	29.93%	1.7
10	20.4 ± 7	23.95%	0.9
11	106.4 ± 141	27.70%	2.6
16	20.1 ± 5	26.55%	1.8
19	7.7 ± 10	27.10%	1.7

Table 4.1. APC, formulated from K_{3h_{5n}}K₃, shows size instability when stored at room temperature (25°C). Size stability of APC over time when stored at room temperature. Size shown with standard deviation and n = 3.

Stability of APC, formulated from $K_{3h_{5n}}K_3$ peptides, were tracked over the course of 19 days at room temperature (**Table 4.1.**), and over the course of 16 days when stored at 4°C (**Table 4.2.**). At room temperature, particle size remains 100-200 nm for the first 9 days. On day 10, the particle size decreases to 20 nm, indicating that particles are breaking down. The Zeta potential also begins decreasing from highly positively (+6.0-25.0 mV) to only +1-3 mV. These results suggest that at room temperature, APC are only stable for about a week, after which they begin to deteriorate. The standard deviations seen for APC stored at room temperature are extremely high. This further suggests that APC are unstable when stored at room temperature, as higher standard deviations indicate there are a broad range of particle sizes in solution.

Day	Size (nm)	Polydispersity	Zeta Potential (mV)
1	259.4 ± 81	28.70%	3.6
2	278.9 ± 102	33.96%	4.7
3	359.8 ± 151	23.06%	0.533
4	123.3 ± 5	28.33%	0.167
5	133.6 ± 20	37.80%	0.033
8	237.5 ± 61	36.26%	0.833
9	168.2 ± 83	18.56%	4.467
10	193.1 ± 70	34.96%	8.867
11	318.0 ± 181	85.23%	3.133
13	84.7 ± 5	37.40%	6.367
14	26.7 ± 26	42.40%	2.667
16	480.0 ± 143	38.63%	0.8

Table 4.2. APC, formulated from $K_{3h_{5n}}K_3$, shows size instability when stored 4°C. Size stability of APC over time when stored at 4°C. Size shown with standard deviation and n = 3.

At 4°C, APC stability does not improve. On day 3, APC size increases from 200-300 nm to 400 nm, indicating particle aggregation. The trends seen in **Table 4.1.** and **Table 4.2.** reveal that when stored at either 4°C or room temperature begin to aggregate together after 3-10 days of storage. These results show that APC are not stable over long periods of time when stored at

room temperature or 4°; when formulated using K₃h_{5n}K₃ peptides. This suggests that when using APC for delivery, they would need to be formulated and used immediately, since aggregation occurs over short periods of time.

Since APC, formulated with K₃h_{5n}K₃ peptides, exhibited poor stability over long periods of time, at both room temperature and 4°C, stability of APC created from K₃h₉K₃ peptides was explored. The increase in hydrophobic residues from FLIVI to FLIVIGSII was hypothesized to potentially increase size stability. At room temperature, stability of K₃h₉K₃ APC appears like that of K₃h_{5n}K₃ APC (**Table 4.3.**). At room temperature, the extended sequence still appears to have stability at room temperature for only about a week, before particle size increases, indicating that APC are beginning to aggregate together and are becoming unstable. After 6 days of storage at room temperature, particle sizes increase from 100-200 nm to 300 nm.

Day	Size (nm)	Polydispersity
1	25.2 ± 3	23.3%
2	147.5 ± 65	49.1%
3	147.9 ± 66	72.5%
5	249.2 ± 34	145%
6	336.5 ± 31	14.5%
7	363.7 ± 65	26.8%
8	177.5 ± 21	149%
9	92.4 ± 73	59.0%
13	161.2 ± 60	36.6%

Table 4.3. APC, formulated from K₃h₉K₃, shows size instability when stored at room temperature (25°C). Each sample was read three times using dynamic light scattering to determine size and polydispersity. The results are the average of those runs, with the standard deviation included in the table for the size, n=3.

Along with stability at room temperature, stability of K₃h₉K₃ APC was examined at 4°C (**Table 4.4.**). Throughout the course of 96 days, the K₃h₉K₃ APC had sizes ranging from 21-400 nm. The standard deviations and polydispersity are lower than previous samples, indicating a narrower range of particle sizes than previous studies. These results indicate that K₃h₉K₃ APC

have slightly increased stability as compared to K₃h_{5n}K₃ APC. But, size stability of APC, whether formulated with either K₃h_{5n}K₃ or K₃h₉K₃ are not stable over long periods of time.

Day	Size (nm)	Polydispersity
1	220.3 ± 36	27.40%
2	22.3 ± 6	22.20%
3	21.8 ± 4	21.20%
5	186.2 ± 38	31.00%
6	227.2 ± 49	14.50%
7	387.1 ± 67	20.00%
8	320.6 ± 44	23.40%
9	225.7 ± 101	23.20%
13	178.8 ± 77	36.30%
14	260.8 ± 137	13.80%
15	435.0 ± 161	16.90%
16	204.2 ± 25	63.50%
18	321.2 ± 46	43.40%
20	349.8 ± 9	13.40%

Table 4.4. Size stability of APC, formulated from K₃h₉K₃, when stored at 4°C, tracked over the course of 96 days. Size stability of extended sequence APC over time when stored at 4°C, tracked over the course of 96 days. Sizes shown with standard deviation and n = 3.

Unfortunately, instability of APC over time is not an ideal characteristic of a delivery system. However, studying the stability of APC using DLS to track changes in size characteristics over time is just one way to look for long-term stability. Future studies could include using NTA to track size distribution profiles of APC over time, giving a better idea of sizes of each individual particle in solution. Forming APC with either genetic material (GFP plasmid or GFP mRNA) and allowing them to incubate for a certain period, at either temperature or 4°C, before using APC to transfect cell lines could also give better insight into the stability of APC as a delivery system.

Chapter 5 - Discussion and Future Work

Discussion

The results of this project reveal that APC show promise as a novel system for genetic material and drug delivery. APC have a simple formulation process, a quality that is important in developing new delivery systems, as current methods, including viral and nonviral vectors, have complex manufacturing steps.^{14,20} When in TFE, peptides formulate α -helical secondary structures, as observed through CD spectral data (**Figure 2.2.**). Removing TFE and rehydrating with pH 2 buffers results in formulation of APC, with random coil secondary structures (**Figure**

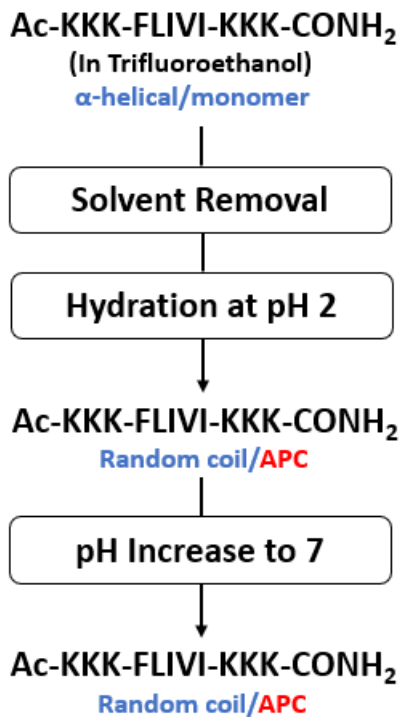


Figure 5.1. APC formulation process. Schematic detailing the formulation process of APC. First, APC are in TFE solution, where they are α -helical in secondary structures. TFE solvent can be removed via vacuum drying and APC can be rehydrated using pH 2 buffers. The pH can be increased to neutral, with APC keeping a random coil secondary structure and small particle size (100-300 nm).

5.1.). Once formulated at pH 2, the pH can be increased without inducing secondary structure or size characteristics alterations.

Suggesting that once capsules have formulated at pH 2, secondary structure becomes locked and resistant to further changes in pH.

These capsules are capable of encapsulation of aqueous dyes and genetic materials, including GFP mRNA, GFP plasmid, and poly I.C. Along with encapsulation abilities, the cationic surface allows for attachment of negatively charged molecules, such as genetic materials, to APC surfaces. Genetic materials both surface-bound and encapsulated within APC can be delivered to cells.

Transfections of both GFP mRNA and GFP plasmid to HEK and BHK cells confirm that ability of APC to deliver these genetic materials into cells. APC transfecting HEK cells with GFP mRNA was confirmed using both confocal microscopy and a Countess™ cell counter. Analyzing transfection using the Countess™ cell

counter allowed for studies into cell viability through trypan blue staining. Trypan blue assays revealed that HEK cell viability was not impacted by treatment of APC as a transfection reagent (Figures 3.8. and 3.9.). Successful transfection reveals that APC can protect genetic materials, as well as penetration of cellular membranes. Studies using RiboGreen™ assays and gel electrophoresis revealed differences in APC with genetic materials encapsulated versus surface bound. Protection of genetic materials and movement through cell membrane are two characteristics needed for successful delivery systems.¹⁴ The results detailed in this paper suggest that APC are a novel delivery system, capable of delivering genetic materials to mammalian cell lines.

The current mechanisms of action that cause capsule formation at acidic pH are currently unknown. However, data suggests that the flanking KKK segments are exposed at the aqueous interface. This would cause the APC surface to be cationic, with the positively charged lysine

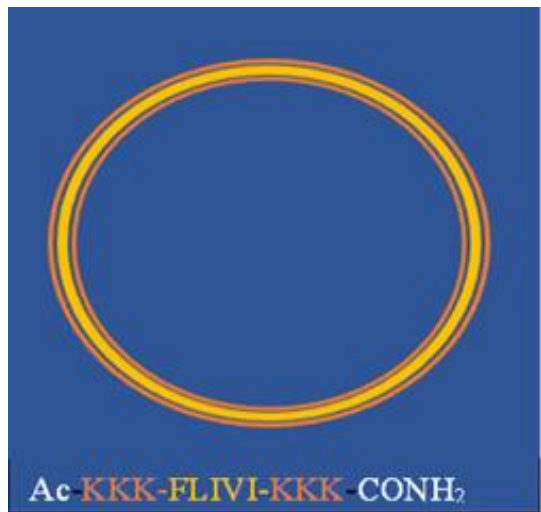


Figure 5.2. Proposed structure of assembled APC in aqueous solvents. Schematic illustrating a proposed formation of APC in aqueous solutions. The flanking KKK segments are exposed to the aqueous solution and the hydrophobic interior segments remain in the interior of the capsules, away from an exposure to the aqueous solutions.

residues being exposed. Zeta potential measurements at acidic pH are consistently positive, indicating the cationic surface of particles. The hydrophobic cores, FLIVI, FLIVIGSII, and IVILF, of APC can be inferred to play a significant role in capsule formation through hydrophobic interactions. Supported by the secondary structures being disrupted by the addition of hydrophobic solvents, such as TFE (Figure 2.2.). This indicates that hydrophobic interactions between the hydrophobic core peptides play a significant role in holding capsules together. A proposed structure of

assembled APC in aqueous solvents is shown in **Figure 5.2**. Based on experimental data, including CD spectra and Zeta potential measurements, the flanking KKK segments on the peptides are exposed to the aqueous solvent. Hydrophobic interactions between hydrophobic interior segments act as a major driving force for capsule formation.

Future Work

One drawback, for APC as a delivery system, is their instability over time, for APC formulated with $K_3h_{5n}K_3$ peptides. However, the APC formulated with $K_3h_9K_3$ showed slightly longer stability over time at 4°C. Compared to BAPC and CAPC, APC are much less stable over long periods of time. Both BAPC and CAPC are stable in temperatures up to 37°C and over the course of a few months.⁴⁹ However, the strong stability of BAPC has manifested problems in their ability to break open and deliver encapsulated solutes into cells.¹⁴ One way to potentially improve the stability of APC would be to create capsules using an equimolar mixture of the $K_3h_{5n}K_3$ and $K_3h_9K_3$ peptides. BAPC contain a mixture of h_5 and h_9 branched peptides (**Figure 1.1**). Since BAPC show significant stability with having a mixture of two peptides, APC may also benefit from using a mixture of the $K_3h_{5n}K_3$ and $K_3h_9K_3$. Future work could explore the characterization, including CD, DLS, and NTA, and delivery capabilities are with the mixture of $K_3h_{5n}K_3$ and $K_3h_9K_3$ peptides.

Studies using fluorescence resonance energy transfer (FRET) pairs could help determine the specific orientation of peptides when they form capsules. FRET pairs are molecules that fluorescence differently when interacting with one another, due to dipole-dipole interactions between an electron donor and acceptor molecule.⁶⁹ Specifically, the FRET pair of tryptophan and 4-cyanophenylalanine could be used, as both molecules can be added onto peptides during synthesis.⁷⁰ Since tryptophan and 4-cyanophenylalanine are a FRET pair, when they interact with

one another the fluorescence will greatly increase, specifically at the excitation wavelength of 270 or 330 nm.⁷⁰ APC could be formulated using a combination of peptides with tryptophan or 4-cyanophenylalanine and assessing them fluorescently. This will determine if peptides align themselves in a way that allows FRET pair interaction, or if they are just aligning themselves randomly to form capsules. Another method to determine how APC form could be to employ computational molecular modeling. Since there are no major differences in protonation state of the APC peptide sequence from pH 2 to pH 7, a question remaining as to why APC formulate nanocapsules at pH 2 and aggregates at pH 7 (**Figure 1.2.**). Computational molecular modeling could allow for exploration into different scenarios in which capsules formulate at acidic pH, giving insight into mechanisms behind APC formation. Molecular modeling has been used previously to model formation of many different types of particles, including chromatosomes, atmospheric molecular clusters, and the self-assembly of protein-complexes.⁷¹⁻⁷³

As mentioned previously, more data are required to explore use of APC as a delivery system. However, one possible clinical application for APC could be for cystic fibrosis (CF) treatment. One major hurdle in treatment of CF is the difficulty for drugs to pass through the thick mucus layers associated with CF airway cells.^{74,75} **Figure 5.3** shows entry of APC, as well as CAPC, containing red dyes into CF airway cells. These results show that both APC and CAPC can penetrate the thick mucus to deliver dyes into underlying CF airway cells. The APC used contained rhodamine 6G dye, as previous studies discussed above confirmed the encapsulation of this dye (**Figure 3.1.**). Since CAPC are able to encapsulate hydrophobic materials, the hydrophobic Nile red dye was used.¹⁴ A control of PBS was used, showing no red fluorescence in the images. Tricaftha® is currently the main treatment for CF patients. Tricaftha® is a combination of three drugs: Ivacaftor, Elexacaftor, and Tezacaftor. A delivery system that

encapsulates and delivers the Tricaftha® directly into cells could help improve treatment, through allowing greater uptake of the drugs. The preliminary results showing entry of APC and CAPC into CF cells, indicating that both peptide-based nanoparticles show promise in aiding delivery of Tricaftha® into CF cells.

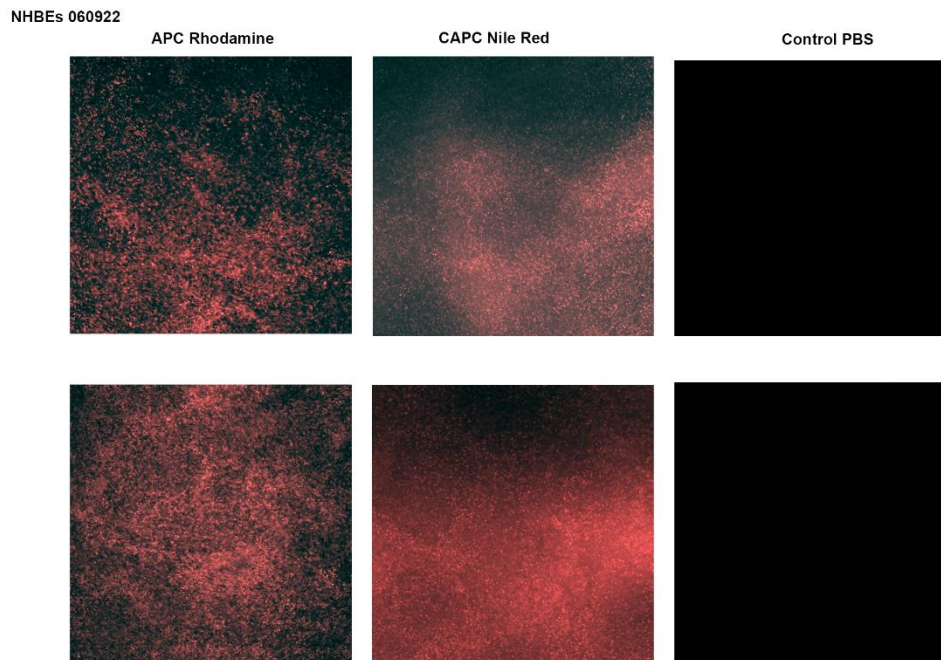


Figure 5.3. Delivery of dyes to cystic fibrosis cells using APC and CAPC. Delivery of Rhodamine 6G dye to cystic fibrosis cells using APC and delivery of Nile Red dye to cystic fibrosis cells using CAPC™. Control of PBS delivered to APC shown as a negative control. Work done at KU Medical Center using their cystic fibrosis cells.

As gene and mRNA therapies, to grow more popular, the demand for delivery systems for these gene therapies and drugs will grow as well.¹⁰ With APC showcasing the ability to deliver mRNA and DNA to eukaryotic cells, which highlights the potential future use of APC as a method to delivery gene therapies. APC positively charged surfaces allow the possibility to encapsulate one material, while simultaneously attaching another, negatively charged, material to APC surfaces. Compared to other delivery methods, APC have simple formulation and production processes. Preparation of APC is cheaper than other methods, such as formulation of liposomes and preparation of viral vectors.^{20,21,28} APC are minimally toxic as they are formulated with peptides. All these qualities make APC a quality delivery system and showcase potential future applications, including drug and mRNA therapy delivery. However, as previously stated, more work focused on APC formation, as well as ways to improve APC stability. Overall, APC show promise as a potential drug or genetic material delivery system in the ever-growing world of nanotechnology.

References

- (1) Shi, J.; Votruba, A. R.; Farokhzad, O. C.; Langer, R. Nanotechnology in Drug Delivery and Tissue Engineering: From Discovery to Applications. *Nano Lett.* **2010**, *10*, 3223–3230. <https://doi.org/10.1021/nl102184c>.
- (2) Contera, S.; Bernardino de la Serna, J.; Tetley, T. D. Biotechnology, Nanotechnology and Medicine. *Emerg. Top. Life Sci.* **2020**, *4*, 551–554. <https://doi.org/10.1042/ETLS20200350>.
- (3) Farokhzad, O. C.; Langer, R. Impact of Nanotechnology on Drug Delivery. *ACS Nano* **2009**, *3* (1), 16–20. <https://doi.org/10.1021/nn900002m>.
- (4) Wong, J.; Mohseni, R.; Hamidieh, A. A.; MacLaren, R. E.; Habib, N.; Seifalian, A. M. Will Nanotechnology Bring New Hope for Gene Delivery? *Trends Biotechnol.* **2017**, *35* (5), 434–451. <https://doi.org/10.1016/j.tibtech.2016.12.009>.
- (5) Dessale, M.; Mengistu, G.; Mengist, H. M. Nanotechnology: A Promising Approach for Cancer Diagnosis, Therapeutics and Theragnosis. *Int. J. Nanomedicine* **2022**, *17*, 3735–3749. <https://doi.org/10.2147/IJN.S378074>.
- (6) Zhang, Y.; Li, M.; Gao, X.; Chen, Y.; Liu, T. Nanotechnology in Cancer Diagnosis: Progress, Challenges and Opportunities. *J. Hematol. Oncol.* **2019**, *12* (137). <https://doi.org/10.1186/s13045-019-0833-3>.
- (7) Kowalski, P. S.; Rudra; Miao, L.; Anderson, D. G. Delivering the Messenger: Advances in Technologies for Therapeutic mRNA Delivery. *Mol. Ther.* **2019**, *27* (4). <https://doi.org/10.1016/j.ymthe.2019.02.012>.
- (8) Chung, Y. H.; Beiss, V.; Fiering, S. N.; Steinmetz, N. F. COVID-19 Vaccine Frontrunners and Their Nanotechnology Design. *ACS Nano* **2020**, *14* (10), 12522–12537. <https://doi.org/10.1021/acsnano.0c07197>.
- (9) Tang, Z.; Zhang, X.; Shu, Y.; Guo, M.; Zhang, H.; Tao, W. Insights from Nanotechnology in COVID-19 Treatment. *Nano Today* **2020**, *36*. <https://doi.org/10.1016/j.nantod.2020.101019>.
- (10) Pan, X.; Veroniaina, H.; Su, N.; Sha, K.; Jiang, F.; Wu, Z.; Qi, X. Applications and Developments of Gene Therapy Drug Delivery Systems for Genetic Diseases. *Asian J. Pharm. Sci.* **2021**, *16*, 687–703. <https://doi.org/10.1016/j.ajps.2021.05.003>.
- (11) Qin, S.; Tang, X.; Chen, Y.; Chen, K.; Fan, N.; Xiao, W.; Zheng, Q.; Li, G.; Teng, Y.; Wu, M.; Song, X. mRNA-Based Therapeutics: Powerful and Versatile Tools to Combat Diseases. *Signal Transduct. Target. Ther.* **2022**, *7* (166). <https://doi.org/10.1038/s41392-022-01007-w>.
- (12) Sahin, U.; Kariko, K.; Tureci, O. mRNA-Based Therapeutics — Developing a New Class of Drugs. *Nat. Rev. Drug Discov.* **2014**, *13*, 759–780. <https://doi.org/10.1038/nrd4278>.
- (13) Feng, R.; Chang, A. C. Y.; Ni, R.; Yin Li, J. C.; Chau, Y. mRNA Delivery and Storage by Co-Assembling Nanostructures with Designer Oligopeptides. *ACS Appl. Biomater.* **2022**, *5*, 3476–3486. <https://doi.org/10.1021/acsbm.2c00397>.
- (14) Barros, S. M.; Whitaker, S. K.; Sukthankar, P.; Avila, A. L.; Gudlur, S.; Warner, M.; Beltrao, E. I. C.; Tomich, J. M. A Review of Solute Encapsulating Nanoparticles Used as Delivery Systems with Emphasis on Branched Amphipathic Peptide Capsules. *Elsevier* **2016**, *596*, 22–42. <http://dx.doi.org/10.1016/j.abb.2016.02.027>.
- (15) Zu, H.; Gao, D. Non-Viral Vectors in Gene Therapy: Recent Development, Challenges, and Prospects. *Am. Assoc. Pharm. Sci.* **2021**, *23* (78).

- (16) Barnard, A. R.; Groppe, M.; MacLaren, R. E. Gene Therapy for Choroideremia Using an Adeno-Associated Viral (AAV) Vector. *Cold Spring Harb. Perspect. Med.* **2015**, *5* (a017293). <https://doi.org/doi:10.1101/cshperspect.a017293>.
- (17) Yan ez-Mun oz, R. J.; Balaggan, K. S.; MacNeil, A.; Howe, S.; Schmidt, M.; Smith, A.; Buch, P.; MacLaren, R. E.; Anderson, P. N.; Barker, S. E.; Duran, Y.; Bartholomae, C.; von Kalle, C.; Heckenlively, J. R.; Kinnon, C.; Ali, R. R.; Thrasher, A. J. Effective Gene Therapy with Nonintegrating Lentiviral Vectors. *Nat. Med.* **2006**, *12* (3).
- (18) Francis, A. I.; Ghany, S.; Gilkes, T.; Umakanthan, S. Review of COVID-19 Vaccine Subtypes, Efficacy and Geographical Distributions. *Postgrad. Med. J.* **2021**, *98*, 389–394. <https://doi.org/10.1136/postgradmedj-2021-140654>.
- (19) Garcia-Montero, C.; Fraile-Martinez, O.; Bravo, C.; Torres-Carranza, D.; Sanchez-Trujillo, L.; Gomez-Lahoz, A. M.; Guijarro, L. G.; Garcia-Honduvilla, N.; Asunsolo, A.; Bujan, J.; Monserrat, J.; Serrano, E.; Alvarez-Mon, M.; De Leon-Luis, J. A.; Alvarez-Mon, M. A.; Ortega, M. A. An Updated Review of SARS-CoV-2 Vaccines and the Importance of Effective Vaccination Programs in Pandemic Times. *Vaccines* **2021**, *9* (433). <https://doi.org/10.3390/vaccines9050433>.
- (20) Srivastava, A.; Mallela, K. M. G.; Deorkar, N.; Brophy, G. Manufacturing Challenges and Rational Formulation Development for AAV Viral Vectors. *J. Pharm. Sci.* **2021**, *110*, 2609–2624. <https://doi.org/10.1016/j.xphs.2021.03.024>.
- (21) van der Loo, J. C. M.; Wright, J. F. Progress and Challenges in Viral Vector Manufacturing. *Hum. Mol. Genet.* **2015**, *25* (R1), R42–R52. <https://doi.org/10.1093/hmg/ddv451>.
- (22) Reichmuth, A. M.; Oberli, M. A.; Jaklenec, A.; Langer, R.; Blankschtein, D. mRNA Vaccine Delivery Using Lipid Nanoparticles. *Ther. Deliv.* **2016**, *7* (5), 319–334. <https://doi.org/10.4155/tde-2016-0006>.
- (23) Wang, C.; Zhang, Y.; Dong, Y. Lipid Nanoparticle–mRNA Formulations for Therapeutic Applications. *Acc. Chem. Res.* **2021**, *54*, 4283–4293.
- (24) Sukthakar, P.; Gudlur, S.; Avila, A. L.; Whitaker, S. K.; Katz, B.; Hiromasa, Y.; Thapa, P.; Gao, J.; Moore, D.; Iwamoto, T.; Chen, J.; Tomich, J. M. Branched Oligopeptides Form Nano-Capsules with Lipid Vesicle Characteristics. *Langmuir* **2013**, *29* (47), 14648–14654. <https://doi.org/doi:10.1021/la403492n>.
- (25) Polack, F. P.; Thomas, S. J.; Kitchin, N.; Absalon, J.; Gurtman, A.; Lockhart, S.; Perez, J. L.; Perez Marc, G.; Roychoudhury, S.; Koury, K.; Li, P.; Kalina, W. V.; Cooper, D.; Frenck, Jr., R. W.; Hammitt, L. L.; Tureci, O.; Nell, H.; Schaefer, A.; Unal, S.; Tresnan, D. B.; Mather, S.; Dormitzer, P. R.; Sahin, U.; Jansen, K. U.; Gruber, W. C. Safety and Efficacy of the BNT162b2 mRNA Covid-19 Vaccine. *N. Engl. J. Med.* **2020**, *383* (27), 2603–2615.
- (26) Ahlawat, J.; Henriquez, G.; Narayan, M. Enhancing the Delivery of Chemotherapeutics: Role of Biodegradable Polymeric Nanoparticles. *Molecules* **2018**, *23* (2157). <https://doi.org/doi:10.3390/molecules23092157>.
- (27) Clark, S. R.; Yong Lee, K.; Lee, H.; Khetan, J.; Chang Kim, H.; Hwa Choi, Y.; Shin, K.; Won, Y.-Y. Determining the Effects of PEI Adsorption on the Permeability of 1,2-Dipalmitoylphosphatidylcholine/Bis(Monoacylglycerol)Phosphate Membranes under Osmotic Stress. *Acta Biomater.* **2018**, *65*, 317–326. <https://doi.org/10.1016/j.actbio.2017.10.027>.

- (28) Fan, Y.; Marioli, M.; Zhang, K. Analytical Characterization of Liposomes and Other Lipid Nanoparticles for Drug Delivery. *J. Pharm. Biomed. Anal.* **2021**, *192* (113642). <https://doi.org/10.1016/j.jpba.2020.113642>.
- (29) Kuang, H.; Ku, S. H.; Kokkoli, E. The Design of Peptide-Amphiphiles as Functional Ligands for Liposomal Anticancer Drug and Gene Delivery. *Adv. Drug Deliv. Rev.* **2016**, *110–111*, 80–101. <https://doi.org/10.1016/j.addr.2016.08.005>.
- (30) Dalby, B.; Cates, S.; Harris, A.; Ohki, E. C.; Tilkins, M. L.; Price, P. J.; Ciccarone, V. C. Advanced Transfection with Lipofectamine 2000 Reagent: Primary Neurons, SiRNA, and High-Throughput Applications. *Methods* **2004**, *33* (2), 95–103. <https://doi.org/10.1016/j.ymeth.2003.11.023>.
- (31) Zhang, H.; De Smedt, S. C.; Remaut, K. Fluorescence Correlation Spectroscopy to Find the Critical Balance between Extracellular Association and Intracellular Dissociation of mRNA Complexes. *Acta Biomater.* **2018**, *75*, 358–370. <https://doi.org/10.1016/j.actbio.2018.05.016>.
- (32) Yu, X.; Liang, X.; Xie, H.; Kumar, S.; Ravinder, N.; Potter, J.; de Mollerat du Jeu, X.; Chesnut, J. D. Improved Delivery of Cas9 Protein/GRNA Complexes Using Lipofectamine CRISPRMAX. *Biotechnol. Lett.* **2016**, *38*, 919–929. <https://doi.org/10.1007/s10529-016-2064-9>.
- (33) Sakurai, Y.; Hatakeyama, H.; Sato, Y.; Hyodo, M.; Akita, H.; Ohga, N.; Hida, K.; Harashima, H. RNAi-Mediated Gene Knockdown and Anti-Angiogenic Therapy of RCCs Using a Cyclic RGD-Modified Liposomal-SiRNA System. *J. Controlled Release* **2014**, *173*, 110–118. <https://doi.org/10.1016/j.jconrel.2013.10.003>.
- (34) Wang, F. S.; Ding, N.; Liu, Z. Q.; Ji, Y. Y.; Yue, Z. F. Ablation Damage Characteristic and Residual Strength Prediction of Carbon Fiber/Epoxy Composite Suffered from Lightning Strike. *Compos. Struct.* **2014**, *117*, 222–233. <https://doi.org/10.1016/j.compstruct.2014.06.029>.
- (35) Raman, S.; Mahmood, S.; Hilles, A. R.; Javed, M. N.; Azmana, M.; Ahmed Saeed Al-Japairai, K. Polymeric Nanoparticles for Brain Drug Delivery - A Review. *Curr. Drug Metab.* **2020**, *21* (9).
- (36) Hussein, W. M.; Cheong, Y. S.; Liu, C.; Liu, G.; Begum, A. A.; Attallah, M. A.; Moyle, P. M.; Torchilin, V. P.; Smith, R.; Toth, I. Peptide-Based Targeted Polymeric Nanoparticles for SiRNA Delivery. *Nanotechnology* **2019**, *30*, 415604. <https://doi.org/10.1088/1361-6528/ab313d>.
- (37) P., R.; V., I. M.; S., K.; F., S.; R., V.; R., Z. Comparison of Transfection Efficiency of Polymer-Based and Lipid-Based Transfection Reagents. *Bratisl. Med. J.* **2018**, *119* (11), 701–705. https://doi.org/10.4149/BLL_2018_125.
- (38) Dehsorkhi, A.; Castelletto, V.; Hamley, I. W. Self-Assembling Amphiphilic Peptides. *J. Pept. Sci.* **2014**, *20*, 453–467. <https://doi.org/10.1002/psc.2633>.
- (39) Lai, Z.; Jian, Q.; Li, G.; Shao, C.; Zhu, Y.; Yuan, X.; Chen, H.; Shan, A. Self-Assembling Peptide Dendron Nanoparticles with High Stability and a Multimodal Antimicrobial Mechanism of Action. *ACS Nano* **2021**, *15*, 15824–15840. <https://doi.org/10.1021/acsnano.1c03301>.
- (40) Natarajan, P.; Tomich, J. M. Understanding the Influence of Experimental Factors on Bio-Interactions of Nanoparticles: Towards Improving Correlation between in Vitro and in Vivo Studies. *Arch. Biochem. Biophys.* **2021**, *694* (2020). <https://doi.org/10.1016/j.abb.2020.108592>.

- (41) Acar, H.; Srivastava, S.; Chung, E. J.; Schnorenberg, M. R.; Barrett, J. E.; LaBelle, J. L.; Tirrell, M. Self-Assembling Peptide-Based Building Blocks in Medical Applications. *Adv. Drug Deliv. Rev.* **2016**, *110–111*, 65–79.
- (42) Guo, Y.; Hu, Y.; Zheng, X.; Cao, X.; Wei, Z.; Zhu, Z.; Zhang, S. Self-Assembled Peptide Nanoparticles with Endosome Escaping Permits for Co-Drug Delivery. *Talanta* **2021**, *221*. <https://doi.org/10.1016/j.talanta.2020.121572>.
- (43) Shah, R. N.; Shah, N. A.; Del Rosario Lim, M. M.; Hsieh, C.; Nuber, G.; Stupp, S. I. Supramolecular Design of Self-Assembling Nanofibers for Cartilage Regeneration. *Proc. Natl. Acad. Sci. USA* **2010**, *107* (8), 3293–3298. <https://doi.org/10.1073/pnas.0906501107>.
- (44) Gudlur, S.; Sukthankar, P.; Gao, J.; Avila, A. L.; Hiromasa, Y.; Chen, J.; Iwamoto, T.; Tomich, J. M. Peptide Nanovesicles Formed by the Self-Assembly of Branched Amphiphilic Peptides. *PLOS ONE* **2012**, *7* (9), e45374.
- (45) Rajagopal, K.; Schneider, J. P. Self-Assembling Peptides and Proteins for Nanotechnological Applications. *Curr. Opin. Struct. Biol.* **2004**, *14*, 480–486. <https://doi.org/10.1016/j.sbi.2004.06.006>.
- (46) Lowik, D. W. P. M.; Leunissen, E. H. P.; van den Heuvel, M.; Hansen, M. B.; van Hest, J. C. M. Stimulus Responsive Peptide Based Materials. *Chem. Soc. Rev.* **2010**, *39*, 3394–3412. <https://doi.org/10.1039/b914342b>.
- (47) Natarajan, P.; Sukthankar, P.; Changstorm, J.; Holland, C. S.; Barry, S.; Hunter, W. B.; Sorenson, C. M.; Tomich, J. M. Synthesis and Characterization of Multifunctional Branched Amphiphilic Peptide Bilayer Conjugated Gold Nanoparticles. *ACS Omega* **2018**, *3*, 11071–11083. <https://pubs.acs.org/doi/10.1021/acsomega.8b01633>.
- (48) Hunter, W. B.; Gonzalez, M. T.; Tomich, J. M. BAPC-Assisted CRISPR/Cas9 System: Targeted Delivery into Adult Ovaries for Heritable Germline Gene Editing (Arthropoda: Hemiptera). *bioRxiv* 478743. <https://doi.org/10.1101/478743>.
- (49) Sukthankar, P.; Whitaker, S. K.; Garcia, M.; Herrera, A.; Boatwright, M.; Prakash, O.; Tomich, J. M. Thermally Induced Conformational Transitions in Nascent Branched Amphiphilic Peptide Capsules. *Langmuir* **2015**, *31* (10), 2946–2955. <https://pubs.acs.org/doi/10.1021/la504381y>.
- (50) Avila, A. L.; Chandrasekar, R.; Wilkinson, K. E.; Balthazor, J.; Heerman, M.; Bechard, J.; Brown, J.; Park, Y.; Dhar, S.; Reeck, G. R.; Tomich, J. M. Delivery of Lethal DsRNAs in Insect Diets by Branched Amphiphilic Peptide Capsules. *J. Controlled Release* **2018**, *273*, 139–147. <https://doi.org/doi:10.1016/j.jconrel.2018.01.010>.
- (51) Natarajan, P.; Roberts, J. D.; Kunte, N.; Hunter, W. B.; Fleming, S. D.; Tomich, J. M.; Avila, A. L. A Study of the Cellular Uptake of Magnetic Branched Amphiphilic Peptide Capsules. *Mol. Pharm.* **2020**, *17*, 2208–2220. <https://dx.doi.org/10.1021/acs.molpharmaceut.0c00393>.
- (52) Sukthankar, P.; Avila, A. L.; Whitaker, S. K.; Iwamoto, T.; Morgenstern, A.; Aspostilidis, C.; Liu, K.; Hanzlik, R. P.; Dadachova, E.; Tomich, J. M. Branched Amphiphilic Peptide Capsules: Cellular Uptake and Retention of Encapsulated Solutes. *Biochem. Biophys. Acta* **2014**, *1838* (9), 2296–2305. <https://doi.org/doi:10.1016/j.bbamem.2014.02.005>.
- (53) Avila, A. L.; Aps, L. R. M. M.; Ploscariu, N.; Sukthankar, P.; Guo, R.; Wilkinson, K. E.; Games, P.; Szoszkiewicz, R.; Alves, R. P. S.; Diniz, M. O.; Fang, Y.; Ferreira, L. C. S.; Tomich, J. M. Gene Delivery and Immunomodulatory Effects of Plasmid DNA Associated with Branched Amphiphilic Peptide Capsules. *J. Controlled Release* **2016**, *241*, 15–24. <http://dx.doi.org/10.1016/j.jconrel.2016.08.042>.

- (54) Barros, S. M.; Sukthankar, P.; Whitaker, S. K.; Coe, M. L.; Hunter, W. B.; Tomich, J. M. Encapsulation of Low Dielectric Oils/Solvents Dispersed in Water by Linear Amphipathic Oligopeptides for Micro/Nano-Carrier Applications. *Langmuir* **2023**.
- (55) Liu, J.; Peng, F.; Kang, Y.; Gong, D.; Fan, J.; Zhang, W.; Qiu, F. High-Loading Self-Assembling Peptide Nanoparticles as a Lipid-Free Carrier for Hydrophobic General Anesthetics. *Int. J. Nanomedicine* **2021**, *2021* (16), 5317–5331. <https://doi.org/10.2147/IJN.S315310>.
- (56) Mo, X.; Hiromasa, Y.; Warner, M.; Al-Rawi, A.; Iwamoto, T.; Rahman, T. S.; Sun, X.; Tomich, J. M. Design of 11-Residue Peptides with Unusual Biophysical Properties: Induced Secondary Structure in the Absence of Water. *Biophys. J.* **2008**, *94*, 1807–1817. <https://doi.org/10.1529/biophysj.107.118299>.
- (57) Greenfield, N. J. Using Circular Dichroism Spectra to Estimate Protein Secondary Structure. *Nat. Protoc.* **2007**, *1* (6), 2876–2890. <https://doi.org/10.1038/nprot.2006.202>.
- (58) Bulheller, B. M.; Rodger, A.; Hirst, J. D. Circular and Linear Dichroism of Proteins. *Phys. Chem. Chem. Phys.* **2007**, *9* (17), 2020–2035. <https://doi.org/10.1039/b615870f>.
- (59) Bhattacharjee, S. DLS and Zeta Potential – What They Are and What They Are Not? *J. Controlled Release* **2016**, *235*, 337–351. <http://dx.doi.org/10.1016/j.jconrel.2016.06.017>.
- (60) Lyu, T. S.; Ahn, Y.; Im, Y.-J.; Kim, S.-S.; Lee, K.-H.; Kim, J.; Choi, Y.; Lee, D.; Kang, E.; Jin, G.; Hwang, J.; Lee, S.; Cho, ung-A. The Characterization of Exosomes from Fibrosarcoma Cell and the Useful Usage of Dynamic Light Scattering (DLS) for Their Evaluation. *PLOS ONE* **2021**, *16* (1). <https://doi.org/10.1371/journal.pone.0231994>.
- (61) Sharma, A.; Cornejo, C.; Mihalic, J.; Geyh, A.; Bordelon, D. E.; Korangath, P.; Westphal, F.; Gruettner, C.; Ivkov, R. Physical Characterization and in Vivo Organ Distribution of Coated Iron Oxide Nanoparticles. *Sci. Rep.* **2018**, *8* (4916). <https://doi.org/10.1038/s41598-018-23317-2>.
- (62) Wilson, D. R.; Green, J. J. Nanoparticle Tracking Analysis for Determination of Hydrodynamic Diameter, Concentration, and Zeta-Potential of Polyplex Nanoparticles. *Biomed. Nanotechnol. Methods Protoc.* **2017**, *1570*, 31–46. https://doi.org/10.1007/978-1-4939-6840-4_3.
- (63) Masri, H.; Raynes, J. K. Nanoparticle Tracking Analysis of β -Casein Nanocarriers. *Protein Nanotechnol.* 303–309.
- (64) Eggeling, C.; Volkmer, A.; Siedel, C. A. M. Molecular Photobleaching Kinetics of Rhodamine 6G by One- and Two-Photon Induced Confocal Fluorescence Microscopy. *ChemPhysChem* **2005**, *6*, 791–804. <https://doi.org/10.1002/cphc.200400509>.
- (65) Hashimoto, J. G.; Beadles-Bohling, A. S.; Wiren, K. M. Comparison of RiboGreen® and 18S RRNA Quantitation for Normalizing Real-Time RT-PCR Expression Analysis. *BioTechniques* **2004**, *36* (1), 54–60.
- (66) Jones, L. J.; Yue, S. T.; Cheung, C.-Y.; Singer, V. L. RNA Quantitation by Fluorescence-Based Solution Assay- RiboGreen Reagent Characterization. *Anal. Biochem.* **1998**, *265*, 368–374.
- (67) Shi, B.; Xue, M.; Wang, Y.; Wang, Y.; Li, D.; Zhao, X.; Li, X. An Improved Method for Increasing the Efficiency of Gene Transfection and Transduction. *Int. J. Physiol. Pathophysiol. Pharmacol.* **2018**, *10* (2), 95–104.
- (68) Louis, K. S.; Siegel, A. C. Cell Viability Analysis Using Trypan Blue: Manual and Automated Methods. *Methods Mol. Biol.* **2011**, *740*. https://doi.org/10.1007/978-1-61779-108-6_2.

- (69) Schneckenburger, H. Förster Resonance Energy Transfer—What Can We Learn and How Can We Use It? *Methods Appl. Fluoresc.* **2019**, *8* (013001). <https://doi.org/10.1088/2050-6120/ab56e1>.
- (70) Ahmed, I. A.; Rodgers, J. M.; Eng, C.; Troxler, T.; Gai, F. PET and FRET Utility of an Amino Acid Pair: Tryptophan and 4Cyanotryptophan. *Phys. Chem. Chem. Phys.* **2019**, *21* (24), 12843–12849. <https://doi.org/doi:10.1039/c9cp02126d>.
- (71) Bharath, M. M. S.; Chandra, N. R.; Rao, M. R. S. Molecular Modeling of the Chromatosome Particle. *Nucleic Acids Res.* **2003**, *31* (14), 4264–4274. <https://doi.org/10.1093/nar/gkg481>.
- (72) Elm, J.; Kubecka, J.; Besel, V.; Jaaskelainen, M. J.; Halonen, R.; Kurten, T.; Vehkamäki, H. Modeling the Formation and Growth of Atmospheric Molecular Clusters: A Review. *J. Aerosol Sci.* **2020**, *149* (105621). <https://doi.org/10.1016/j.jaerosci.2020.105621>.
- (73) Amin, S.; Barnett, G. V.; Pathak, J. A.; Roberts, C. J.; Sarangapani, P. S. Protein Aggregation, Particle Formation, Characterization & Rheology. *Curr. Opin. Colloid Interface Sci.* **2014**, *19* (5), 438–449. <https://doi.org/10.1016/j.cocis.2014.10.002>.
- (74) Lee, J.-A.; Cho, A.; Huang, E. N.; Xu, Y.; Quach, H.; Hu, J.; Wong, A. P. Gene Therapy for Cystic Fibrosis: New Tools for Precision Medicine. *J. Transl. Med.* **2021**, *19* (452). <https://doi.org/10.1186/s12967-021-03099-4>.
- (75) Rafeeq, M. M.; Murad, H. A. S. Cystic Fibrosis: Current Therapeutic Targets and Future Approaches. *J. Transl. Med.* **2017**, *15* (84). <https://doi.org/10.1186/s12967-017-1193-9>.